Control-Oriented Modeling, Simulation, and Predictive Control of District Heating Networks

Lorenzo Nigro, *Graduate Student Member, IEEE*, Alessio La Bella, *Member, IEEE*, Francesco Casella, *Member, IEEE*, and Riccardo Scattolini

***Abstract*— District heating networks (DHNs) are recognized as pivotal infrastructures to reduce the carbon footprint of the heating sector. However, their large-scale dimension and the involved nonlinear dynamics lead to significant issues regarding their modeling and optimal control. Tackling these challenges, two dynamic DHN modeling frameworks are presented: a detailed simulation model and a control-oriented one. The simulation model allows the development of lightweight dynamic DHN simulators, accurately represents the main system dynamics in reduced computational time, and is well-suited for testing online control algorithms. This model is leveraged to develop a simulation library for DHN systems in the Modelica environment, named *DHN4Control*, freely distributed with this article in Nigro (2023). Then, a methodology for deriving a control-oriented DHN model is presented, suitable for designing a nonlinear model predictive control (NMPC) regulator, ensuring computationally efficient and cost-effective regulation while respecting operative constraints. The developed modeling and control methods are tested in simulation considering as benchmark a Test Facility district heating plant located at Ricerca sul Sistema Energetico - RSE S.p.A. in Milan (Italy), showing promising results in terms of modelling accuracy, computational efficiency and energy savings.**

***Note to Practitioners*—The dimension and complexity of multi-producer district heating networks (DHN) make their modeling, simulation, and online optimization challenging tasks. This work proposes a solution for district heating networks efficient simulation and optimal control design. The detailed explanations of the modelling equations and the use of open source software increase results replicability for practitioners. The simulation-oriented model comes with a lightweight simulation library, readily available at Nigro (2023). The control-oriented model is reusable on generic multi-producer district heating networks, for computationally efficient optimization-based control design. The optimal control is able to manage thermal generators and storages to minimize DHN operational costs while respecting operational constraints over the whole thermal network. The proposed solution is tested in simulation considering a real-world DHN plant currently under construction at Ricerca sul Sistema Energetico - RSE S.p.A in Milan (Italy). The simulation results show the cost saving performances of optimal controllers developed with the proposed model. Overall, by using the proposed solution, one can achieve faster simulation times and ease the burden of optimal control modelling for the development of an optimal-based control strategy for cost-effective DHN operation.**

***Index Terms*— District heating network, model predictive control, control-oriented model, energy efficiency.**

Received 12 June 2024; revised 8 August 2024; accepted 8 September 2024. This article was recommended for publication by Associate Editor R. Carli and Editor Q. Zhao upon evaluation of the reviewers' comments. The work of Lorenzo Nigro was supported by the Research Fund for the Italian Electrical System under the Contract Agreement between Ricerca sul Sistema Energetico S.p.A. and the Ministry of Economic Development-General Directorate for the Electricity Market, Renewable Energy and Energy Efficiency, Nuclear Energy. The work of Alessio La Bella and Riccardo Scattolini was supported by the Next-Generation European Union (EU) (Italian Piano Nazionale di Ripresa e Resilienza (PNRR)-M4 C2, Invest 1.3-D.D. 1551.11-10-2022, PE00000004) under Grant CUP MICS D43C22003120001. *(Corresponding author: Alessio La Bella.)*

Lorenzo Nigro is with the Dipartimento di Elettronica, Informazione e Bioingegneria, Politecnico di Milano, 20133 Milan, Italy, and also with Ricerca sul Sistema Energetico (RSE) S.p.A., 20134 Milan, Italy (e-mail: lorenzo.nigro@polimi.it).

Alessio La Bella, Francesco Casella, and Riccardo Scattolini are with the Dipartimento di Elettronica, Informazione e Bioingegneria, Politecnico di Milano, 20133 Milan, Italy (e-mail: alessio.labella@polimi.it; francesco.casella@polimi.it; riccardo.scattolini@polimi.it).

Color versions of one or more figures in this article are available at https://doi.org/10.1109/TASE.2024.3460173.

Digital Object Identifier 10.1109/TASE.2024.3460173

I. Introduction

HEATING and cooling requirements for residential, commercial, and industrial buildings in Europe account for nearly 50% of their total energy demand, the majority of which is supplied by fossil fuels [2]. In response to the European 2050 targets for net zero greenhouse gas emissions and the global push towards decarbonization, district heating networks (DHNs) have emerged as a promising solution, given their environmental and economic benefits to society [3], [4]. Consequently, the European Union intends to cover at least 50% of the heating demand of most European countries with DHN systems by 2050 [5].

DHNs are plants for the generation, distribution, and consumption of heat which is usable for indoor heating and domestic hot water. They involve thermal generators (e.g., heat pumps, boilers), storages (e.g., insulated tanks), and loads (e.g., households, buildings). The generated heat transfers to loads through water flowing in the supply pipeline. Then, water flows back to the generators via the return pipeline to reheat. Based on the topology, DHNs' structure can be single producer, i.e., where thermal generators lay in a single heating node, or multi-producer, in the presence of generation distributed over the network [6]. Nowadays, most DHN plants are operated by simple rule-based control strategies, which are unable to exploit networks' full potential and cause increased thermal losses and operational costs. The motivation of this study is to unlock district heating network efficiency through optimization-based control strategies [7], [8]. Nevertheless, modeling complex and large-scale DHNs implies two key challenges: suitable dynamical simulator design, which is a necessary tool for testing control strategies' performances and

proper system management, as well as the networks' optimal operation point computation, e.g., leveraging Model Predictive Control (MPC) strategies. Two models shall be developed to answer this needs.

A. Related Work

Concerning the simulation of DHN, the mathematical modeling describing single-producer DHN in [9] is accomplished using partial differential equations, whereas in [10] is done through a port-Hamiltonian approach. Multi-producer DHN models stability and passivity properties are analyzed in [11] and [12]. Nonetheless, some modeling aspects are omitted in the mentioned references, e.g., pipeline metal walls' thermal inertia, pipe sections' variation, or thermal storage dynamics.

A precise DHN model is pivotal to accurately simulate thermo-hydraulic dynamical behavior [13]. DHN simulators can be based on detailed modeling libraries for thermo-hydraulic systems, for example, the *ThermoPower* library developed in Modelica [14], [15] or the MATLAB toolbox *Simscape* [16], [17]. Nevertheless, these simulation environments require numerous physical parameters that may be unavailable. Moreover, they model dynamics that are less relevant for DHNs (e.g., fluid phase transition, pressure-varying, or temperature-varying heat coefficients) leading to additional computational effort and slower simulations, often without useful information return. Consequently, testing and tuning optimization-based regulators through the mentioned simulation environments becomes increasingly intensive and not practical.

Concerning the design of MPC regulators for DHN systems, some works have been proposed in the literature. For instance, a stabilizing MPC approach is proposed in [18], however not considering the cost-effective DHN management and applied to a small-size exemplary benchmark. In fact, the large-scale dimension and nonlinear dynamics of highly detailed DHN models affect the optimal control problem design and lead to computational issues from the optimization perspective. In this context, [9] describes an optimization scheme for DHNs; nonetheless, it suffers from large-scale nonlinearities and is solvable only using a single-step prediction horizon. On the other hand, in [19], a particle swarm optimization algorithm is employed to solve the DHN control problem, however, the authors states that the resulting computational burden is not admissible for practical implementation.

Most of the exiting solutions to decrease the computational complexity of MPC regulators for DHN systems, most of them rely on simplified models. For instance, in [20], [21], [22], and [23], the MPC regulator employs models based on thermal static power balances, i.e., they neglect temperature dynamics over network pipelines. In fact, temperature dynamics are essential in DHN control design for two main reasons. First, the water temperature must respect different operative constraints over the network (e.g., the supply temperature of all loads must exceed a threshold for proper operation [9], [11]). Second, the generation costs and heat loss minimization require temperature dynamics knowledge to account for the intrinsic water pipelines' thermal inertia. Thus, temperature modelling appear in other MPC solutions, leveraging different simplifying assumptions to reduce complexity. For instance, in [24], authors assume fixed transport delays and water flow over the network. In [25], solely the return network temperature is considered using a linear model, whereas, in [26], water supply temperature is the same across all loads, i.e., neglecting network thermal losses. In [27], bi-directional power flows are also considered, and the complexity is reduced by neglecting delays, heat losses, and the thermal inertia of the pipeline network. Nevertheless, none of these solutions enable to properly consider heating network inertia and constraints.

On the other hand, data-driven models have been also proposed in the literature for DHN systems, as in [8], [28], [29], [30], and [31]. In this context, Gaussian data-based models are employed in [32] for modelling thermal dynamics in DHN systems, whereas data-driven linear models are exploited in [33]. The drawback of these data-based approaches is that they neglect any available physical knowledge of the DHN. This last aspect has been addressed in [34], where a physics-informed data-based model is proposed for DHN systems, combining data and the available physical knowledge, i.e., the network topology. Nevertheless, data-based modelling methods rely on large operational datasets highly exciting system dynamics, which are hardly available in real DHN applications.

B. Main Contribution

The above discussion motivates the necessity of developing novel control-oriented DHN models, which must be computationally-efficient and accurate enough to properly represent network thermal dynamics. This control-oriented modelling must enable the design of predictive control strategies capable of effectively optimizing DHN operations, and guaranteeing to respect all required network constraints. On the other hand, lightweight and DHN-oriented simulation environments are also required, for testing and tuning the designed optimization-based controllers. These challenges are solved through the following main contributions of this work.

- *DHN modeling for computationally-efficient and accurate simulators:* As discussed, existing works on detailed DHN models neglect fundamental elements, e.g., [9], [10], [11], [12], whereas other frameworks involve demanding and slow simulations being not focused on DHN systems, e.g., [14] and [15]. Thus, this paper formulates a complete multi-producer DHN model, featuring all main elements (e.g, generators, loads, storages, pipes, pipe fitting, etc.). The model considers the typical DHN operation to capture its relevant dynamics and neglects less relevant phenomena in DHN systems (e.g., fluid phase transition), enabling the design of a fast and accurate dynamic simulation environment, suited for testing online optimization-based controllers. The resulting simulation library, called *DHN4Control*, is developed in Modelica and freely distributed with this work [1]. The *DHN4Control* library can be used

for any DHN configuration and it is tested both with experimental data and against other simulation libraries, e.g., [15], showing to be accurate and computationally lighter.

- *DHN control-oriented model and nonlinear predictive control design:* Existing control strategies for DHN systems rely on highly complex models unsuitable for optimal predictive control, e.g., [9], [10], [11], [12]. Because of this, other control approaches have relied on oversimplifying assumptions, but these are incapable of exploiting DHN thermal inertia, e.g., [20], [21], [22], [23], [24], [25], [26], [27]. Some data-based controllers for DHN also exists, however they necessitate large amount of exciting operational data, which is not always feasible in practice, e.g., [28], [29], [30], [31], [32], [33], [34]. In view of this, another contribution of the work consists in developing a novel DHN control-oriented modelling with enhanced dynamical accuracy and computational efficiency, recovered from the detailed simulation one through new model reduction methods. Among these, we here mention: the substitution of pressure modeling with equivalent, but light-way, algebraic relationships enforced at each network closed path, and the reduced pipe modelling combining pipe wall and flow thermal dynamics. The presented control-oriented model achieves enhanced modeling accuracy when compared with the detailed DHN simulation model, but with a significant lower number of variables (around 90% reduction), paving the way for the design of a computationally-efficient Nonlinear Model Predictive Control (NMPC) regulator, optimizing large-scale DHN plants in few seconds. The designed NMPC regulator enables to minimize generation costs and to increase system efficiency by properly exploiting DHN thermal inertia, while ensuring constraints respect over the whole thermal network.

The developed methods are tested through detailed simulators considering a real DHN benchmark, hereafter named: "Thermal Test Facility", which is currently under construction at the research center Ricerca sul Sistema Energetico - RSE SpA, Milan, Italy. For the sake of completeness, the obtained performances are also evaluated on a larger benchmark taken from the literature, i.e., the AROMA district heating network [9]. The solution obtains high modelling accuracy, reduced computational complexity, and the resulting NMPC regulators achieve up to 15% of cost reduction compared to standard rule-based control strategies.

C. Paper Outline

The paper is organized as follows. In Section II, the DHN modeling is described in detail together with the developed simulation library. In Section III, the DHN control-oriented model, the reduction procedure to obtain it, and the NMPC regulator design are discussed. Additionally, Section IV displays the numerical results regarding the developed modeling and control methods applied to the Thermal Test Facility. The conclusions are in Section V.

D. Notation

Let $\mathbb{R}$ denote the set of real numbers, $\mathbb{R}_{\geq 0}$ the set of positive or null real numbers including zero, and $\mathbb{R}_{>0}$ the set of strictly positive real numbers. Moreover, let $\mathbb{N}$ denote the set of natural numbers. Given a matrix A, $A \in \mathbb{R}^{n,m}$ indicates that it has n rows and m columns and all its entries are real numbers. Given a vector a, $a \in \mathbb{R}^n$ indicates that it has n rows and one column, and all its entries are real numbers. Given a matrix A and a vector a, their transpose are denoted with A' and a', respectively. Given two vectors of variables $x, y \in \mathbb{R}^n$, the inequalities among the two, e.g., $x > y$, are intended element-wise. For a vector $x \in \mathbb{R}^n$, the vectors of the corresponding upper and lower bounds are $\overline{x} \in \mathbb{R}^n$ and $\underline{x} \in \mathbb{R}^n$, respectively, with $\overline{x} > \underline{x}$.

II. Modelling of District Heating Networks

DHNs are large-scale systems governed by nonlinear Partial Differential Equations (PDE). These PDE describes the dynamical relationships among water mass flows, pressures, and temperatures [9]. A typical DHN is composed of the following main elements, also depicted in Figure 1(a):

- a supply network, where water at high temperature flows from thermal generators to loads;
- a return network, where water flows back to thermal generators after having transferred heat to loads;
- thermal generation, which heat the water supplied by the return network through local units (e.g., boilers) and then pump it back into the supply distribution network;
- thermal loads, which absorb heat from the water in the supply distribution network through a local heat exchanger and then inject it back into the return distribution network;
- thermal energy storages (TESs), which are insulated water tanks with constant mass connected to the supply and return distribution network. TESs typically store high-temperature water and deliver it when convenient.

In addition to these main elements, a DHN comprises valves, pumps, and pipes, which will be modeled in the following relying on their physical equations. Before formulating the DHN model, we state a few assumptions leading to a physical model with reasonable complexity and accuracy for the design and test of control systems. Specifically, the stated assumptions are valid in a typical operating range for high-temperature DHNs, i.e., with water pressure between 2 and 10 bar and water temperatures between 60 and 90°C, [35].

Assumption 1: Water is assumed incompressible and with constant specific heat. The water density and specific heat values derive from IAPWS-IF97 standard[1] and are equal to their average value in the considered operating range. Specifically, the following values are considered $\rho = 998\,\mathrm{kg/m^3}$ and $c = 4185\,\mathrm{J/kg\ K}$.

Assumption 2: Each pipe is assumed to have rigid metal walls and a constant circular section. Cross-sectional area variations among pipes are modeled as lumped in specific points of the DHN, commonly named pipe fittings.

[1] http://www.iapws.org/relguide/IF97-Rev.html

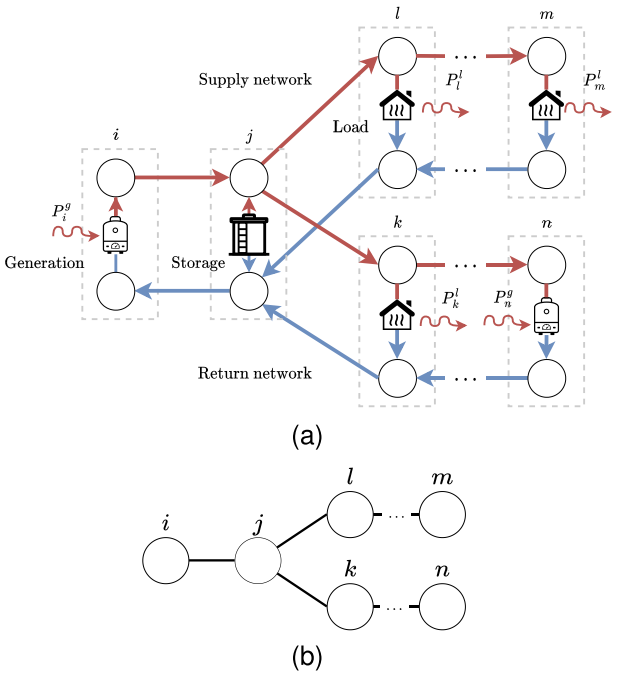

Fig. 1. (a) Schematic of a DHN with supply and return distribution network, respectively in red and blue, a thermal generator at node i, thermal loads at nodes l and k, and a thermal storage at node j. (b) Equivalent graph representation of the DHN.

Assumption 3: Pressure transients are assumed instantaneous, as pressure waves travel in the fluid with the speed of sound, whereas temperature variations travel with the flow velocity [36]. Hence, inertial and compressibility effects in momentum balance equations are neglected, reducing pressure modeling to algebraic nonlinear equations.

Assumption 4: For notational simplicity, the supply and return distribution networks are assumed to have the same topology, as typical in DHNs [11], [37].

Consider the DHN reported in Figure 1(a). Given Assumption 4, a DHN can be represented with a single undirected, connected, and planar graph $G = (\mathcal{N}, \mathcal{E})$, as shown in Figure 1(b), where $\mathcal{N}$ is the set of nodes of the DHN and $\mathcal{E}$ the set of edges, representing physical interconnections among nodes.

Each node $i \in \mathcal{N}$ represents a significant element in the DHN, e.g., a thermal generator, a storage, a load, or a junction among multiple pipes. Specifically, the set of generation nodes is denoted as $\mathcal{G} \subset \mathcal{N}$, the set of load nodes as $\mathcal{L} \subset \mathcal{N}$, the set of thermal storage nodes as $\mathcal{Z} \subset \mathcal{N}$. Note that, for the sake of simplicity, it is here assumed that these sets do not have common nodes, i.e., $\mathcal{G} \cap \mathcal{L} \cap \mathcal{Z} = \emptyset$, meaning that if two elements are connected (e.g., a generator and a storage), two fictitious connected nodes are defined. Moreover, specific variables describing the water state are introduced for each node of the DHN: *i)* the water mass flow q $[\mathrm{kg/s}]$, *ii)* its pressure p [Pa], and *iii)* its temperature T [°C]. Referring to Figure 1(a), all nodes $i \in \mathcal{N}$ interface with the supply and the return pipelines; hence, they require two sets of variables defined as: $(q_i^s,\ p_i^s,\ T_i^s)$ describing the net water flow, pressure, and temperature at the supply distribution network connection, and $(q_i^r,\ p_i^r,\ T_i^r)$ describing the same quantities at the return. The superscripts s and r specify if variables and parameters belong to the supply or the return respectively; for the sake of compactness, a generic superscript v with $v \in \{s, r\}$ represents both.

Each edge $(i, j) \in \mathcal{E}$ interconnecting node i and j physically represents either a distribution pipe (see Figure 2) or a pipe fitting, i.e., a lumped-element where the pipe section changes (see Figure 3). Thus, define as $\mathcal{E}_P$ the set of edges representing distribution pipes, and as $\mathcal{E}_F$ the set of edges representing pipe fitting, where $\mathcal{E} = \mathcal{E}_P \cup \mathcal{E}_F$. Moreover, $\forall (i, j) \in \mathcal{E}$, q_{ij}^v and q_{ji}^v describe the water flow where $q_{ij}^v \geq 0$ and $q_{ji}^v \leq 0$ if the water flows from node i to j, whereas $q_{ji}^v > 0$ and $q_{ij}^v < 0$ if the water flows from node j to i; the same holds at the supply $(v = s)$ and the return $(v = r)$ network.

Please refer to Table I for the description of the main variables and parameters used for the DHN model. Note that the superscript v is used for some parameters, which can be referred either to the supply $(v = s)$ or the return $(v = r)$ network. Hereafter, DHN edges modelling is first described, then DHN nodes are modelled.

A. Distribution Network Model

1) Pipe Model: Pipes are modelled featuring the one-dimensional finite-volume method [9]. This model consists of the spatial discretization in mono-dimensional sections with boundaries orthogonal to the water flow direction, as reported in Figure 2. The pipe's sections comprise a lumped dynamical temperature model that expresses energy balances and exchanges among adjacent sections and their pipe walls.

Supply and return pipes at the edge $(i, j) \in \mathcal{E}_P$ are characterized by a vertical displacement y_{ij}^v, a total length L_{ij}^v, internal radius r_{ij}^v, and external radius r_{ij}^{vm}, as depicted in Figure 2. Given the finite volume method, each supply and return pipe in the edge (i, j) is divided into n_{ij}^v sections with boundaries orthogonal to the water flow direction, each one of length $l_{ij}^v = L_{ij}^v / n_{ij}^v$ and volume $v_{ij}^v = l_{ij}^v \pi {r_{ij}^v}^2$. The water temperature of the generic kth pipe section is denoted with $T_{ij,k}^v$, whereas the temperature of the pipe wall at that section is $T_{ij,k}^{vm}$, with $k \in \{1, \ldots, n_{ij}^v\}$. Thus, the dynamic model of the water temperature for the kth pipe section is

$$
\begin{aligned}
c\,\rho\, v_{ij}^v\, \dot{T}_{ij,k}^v(t) = {} & 2\pi r_{ij}^v\, l_{ij}^v\, U_{ij}^m\, (\, T_{ij,k}^{vm}(t) - T_{ij,k}^v(t)\,) \\
& + c\, q_{ij}^v(t) \begin{cases} T_{ij,k-1}^v(t) - T_{ij,k}^v(t) & \text{if } q_{ij}^v(t) \geq 0 \\ T_{ij,k}^v(t) - T_{ij,k+1}^v(t) & \text{if } q_{ij}^v(t) < 0 \end{cases}
\end{aligned} \tag{1}
$$

for each $k \in \{1, \ldots, n_{ij}^v\}$ and $v \in \{s, r\}$. Moreover, by imposing $T_{ij,0}^v(t) = T_i^v(t)$ and $T_{ij,n_{ij}^v+1}^v(t) = T_j^v(t)$, one can express the interface of each pipe (i, j) to the nodes i and j at its extremes (see Figure 2). The left-hand side of equation (1) corresponds to the derivative of the thermal energy in the kth section, whereas the right-hand side includes the heat transfer towards the pipe metal wall, depending on the conduction area and the heat transfer coefficient U_{ij}^m, and the thermal energy exchanged with the adjacent sections due to transport

TABLE I
MAIN VARIABLES AND PARAMETERS

Name	Description	Unit
c	Water specific heat	[J/kg/K]
g	Gravitational acceleration	[m/s^2]
p	Water pressure	[bar]
q	Water mass flow rate	[kg/s]
ρ	Water density	[kg/m^3]
c_f	Pipe fanning coefficient	[-]
c_m	Pipe metal specific heat	[J/m$^3\cdot$ s]
L^v_{ij}	Pipe ij length	[m]
n^v_{ij}	Pipe ij number of sections	[-]
q^v_{ij}	Pipe ij mass flow rate	[kg/s]
r^v_{ij}	Pipe ij internal radius	[m]
r^{vm}_{ij}	Pipe ij external radius	[m]
$T^v_{ij,k}$	Pipe ij kth section water temperature	[°C]
$T^{vm}_{ij,k}$	Pipe ij kth section metal temperature	[°C]
T^e_{ij}	Pipe ij external temperature	[°C]
U^{vm}_{ij}	Pipe ij heat transfer coefficient water-metal	[W/K·m^2]
U^{ve}_{ij}	Pipe ij heat transfer coefficient metal-ambient	[W/K$\cdot$ m^2]
y^v_{ij}	Pipe ij vertical displacement	[m]
k^v_1, k^v_2	Pipe fitting ij friction coefficients	[-]
A^l_i	Load i Valve opening area	[m^2]
θ^l_i	Load i valve opening	[-]
P^l_i	Load i thermal power	[W]
q^l_i	Load i mass flow rate	[kg/s]
T^l_i	Load i output temperature	[°C]
P^g_i	Generator i thermal power	[W]
H^z_i	TES i height	[m]
n^z_i	TES i number of sections	[-]
q^z_i	TES i mass flow rate	[kg/s]
r^z_i	TES i base radius	[m]
$T^z_{i,k}$	TES i kth section water temperature	[°C]
$T^{z\,e}_i$	TES i external temperature	[°C]
α	TES i dispersion coefficient	[W/K·m^2]
κ	TES i conduction coefficient	[W/K·m^2]

phenomena. For compactness, introduce the vectors

$$\mathbf{T}^v_{ij} = \left[T^v_{ij,1},\ \ldots,\ T^v_{ij,n^v_{ij}}\right]', \quad \mathbf{T}^{vm}_{ij} = \left[T^{vm}_{ij,1},\ \ldots,\ T^{vm}_{ij,n^v_{ij}}\right]',$$

and the matrices $\Phi, \Psi \in \mathbb{R}^{n^v_{ij}, n^v_{ij}}$, defined as

$$\Phi_{ij} = \begin{cases} -1 & \text{if } i = j \\ 1 & \text{if } j = i-1 \wedge i > 1 \\ 0 & \text{otherwise} \end{cases}, \tag{2a}$$

$$\Psi_{ij} = \begin{cases} -1 & \text{if } i = j \\ 1 & \text{if } j = i+1 \wedge i < n_{ij} \\ 0 & \text{otherwise} \end{cases}, \tag{2b}$$

and the vectors $\boldsymbol{\delta} = [1, 0, \ldots, 0]'$ and $\boldsymbol{\omega} = [0, \ldots, 0, 1]'$, with $\boldsymbol{\delta}, \boldsymbol{\omega} \in \mathbb{R}^{n^v_{ij}}$. Thus, equation (1) can be rewritten as

$$\begin{aligned} c\,\rho\, v^v_{ij}\dot{\mathbf{T}}^v_{ij}(t) &= 2\pi r^v_{ij}\, l^v_{ij}\, U^m_{ij}(\mathbf{T}^{vm}_{ij}(t) - \mathbf{T}^v_{ij}(t)) \\ &\quad + c\, q^v_{ij}(t)\begin{cases} \Phi\,\mathbf{T}^v_{ij}(t) + \boldsymbol{\delta} T^v_i(t) & \text{if } q^v_{ij}(t) \geq 0 \\ \boldsymbol{\omega} T^v_j(t) - \Psi\,\mathbf{T}^v_{ij}(t) & \text{if } q^v_{ij}(t) < 0\,, \end{cases} \end{aligned} \tag{3a}$$

for each $v \in \{s, r\}$.

Another crucial factor to consider for DHN analysis is the pipe's metal wall thermal dynamic as it can significantly impact the water temperature dynamical behavior, as discussed in [13]. Consider the pipe external radius r^{vm}_{ij} and wall section

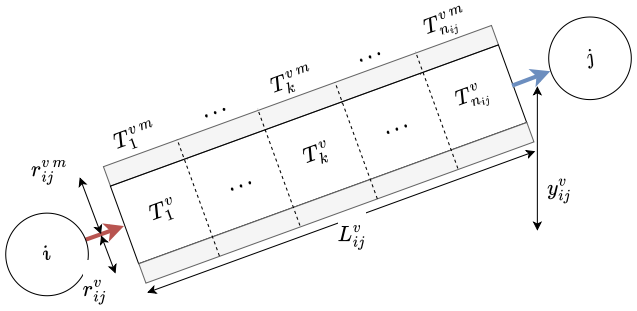

Fig. 2. One-dimensional, finite-volume method, and pipe's parameters and variables.

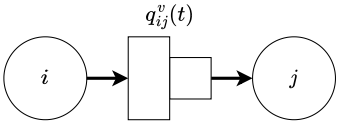

Fig. 3. Pipe fitting for changes in pipe's section.

volume $v^{vm}_{ij} = l^v_{ij}\pi\left((r^{vm}_{ij})^2 - (r^v_{ij})^2\right)$. Then, the pipe metal wall temperature model is

$$\begin{aligned} c_m\,\rho_m\, v^{vm}_{ij}\,\dot{\mathbf{T}}^{vm}_{ij}(t) &= 2\pi r^v_{ij}\, l^v_{ij}\, U^m_{ij}\,(\,\mathbf{T}^v_{ij}(t) - \mathbf{T}^{vm}_{ij}(t)\,) \\ &\quad - 2\pi r^{vm}_{ij}\, l^v_{ij}\, U^e_{ij}\left(\mathbf{T}^{vm}_{ij}(t) - \mathbb{1}\, T^{v,e}_{ij}(t)\right), \end{aligned} \tag{3b}$$

for each $v \in \{s, r\}$. The left-hand side of the equation expresses the derivative of the pipe wall section thermal energy; instead, the right-hand side includes the energy exchange with the flowing water and with the external environment, supposed to be at temperature $T^{v,e}_{ij}$, which may correspond to the ground temperature as DHN pipes commonly lay underground.

The pressure drop across pipes is modelled through Fanning's formula [38], which reads as

$$p^v_i(t) - p^v_j(t) = \rho g y^v_{ij} + \rho\begin{cases} c_f\dfrac{L^v_{ij}}{r^v_{ij}}\left(\dfrac{q^v_{ij}(t)}{\rho\pi {r^v_{ij}}^2}\right)^2 & \text{if } q^v_{ij}(t) \geq 0, \\ -c_f\dfrac{L^v_{ij}}{r^v_{ij}}\left(\dfrac{q^v_{ij}(t)}{\rho\pi {r^v_{ij}}^2}\right)^2 & \text{if } q^v_{ij}(t) < 0, \end{cases} \tag{4}$$

for each $v \in \{s, r\}$, where c_f is the Fanning coefficient, and g is the gravitational acceleration.

2) Pipe Fitting Model: As previously discussed, assume lumped cross-section variations and represent them with an edge $(i, j) \in \mathcal{E}_F$ in the supply and return networks, as shown in Figure 3. Exploiting Bernoulli's equation [39], the pressure drop at each pipe fitting edge $(i, j) \in \mathcal{E}_F$ is

$$p^v_i(t) - p^v_j(t) = \frac{q^v_{ij}(t)^2}{2\rho}\begin{cases} k^v_{1,ij} & \text{if } q^v_{ij}(t) \geq 0 \\ -k^v_{2,ij} & \text{if } q^v_{ij}(t) < 0 \end{cases}, \tag{5}$$

where $v \in \{s, r\}$, and $k^v_{1,ij}$ and $k^v_{2,ij}$ are fixed tabulated friction coefficients depending on the pipe fitting geometry (e.g., cross-section variation, contraction angles, etc.). More details on

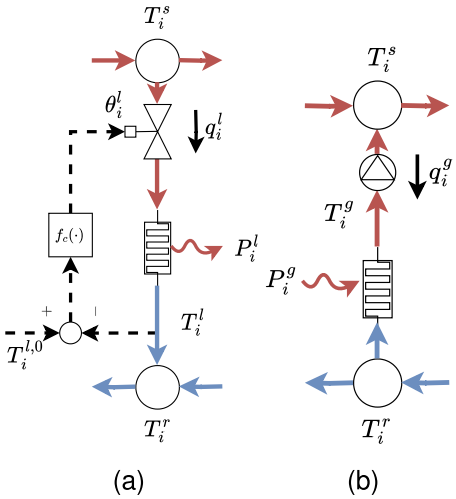

Fig. 4. (a) Generic load structure. (b) Generator node structure.

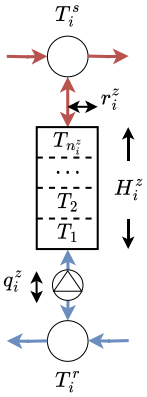

Fig. 5. Schematic of a thermal energy storage.

pipe fitting coefficients related to their specific geometry are available in [40]. Moreover, assume no temperature losses occur across pipe fittings, i.e.,

$$T_i^v = T_j^v, \tag{6}$$

with $v \in \{s, r\}$, and $(i, j) \in \mathcal{E}_F$.

B. Node Models

As anticipated, most DHNs' components belong to one of three node categories: thermal loads, generators, and storages. The first two categories involve static models as their time constants are negligible compared to those of the network transport dynamics. On the other hand, the thermal storage models are dynamic as they show significant thermal inertia.

1) Load Model: Each load node $i \in \mathcal{L}$ connects the supply and the return distribution network, absorbing a water flow $q_i^l \in \mathbb{R}_{\geq 0}$ from the supply network through a locally regulated valve, as depicted in Figure 4(a). The absorbed water goes through the load heat exchanger, which extracts thermal power $P_i^l \geq 0$. Thus, it holds that

$$P_i^l(t) = c\, q_i^l(t)\, (T_i^s(t) - T_i^l(t))\,, \tag{7}$$

where $T_i^l(t)$ is the output water temperature at the load heat exchanger. As proposed in [41], loads are temperature-controlled, implying that the water flow q_i^l is regulated through the local valve to track a reference $T_i^{l,0}$ for the output water temperature. This is modelled as

$$\dot{\theta}_i^l(t) = f_c(\theta_i^l(t),\ T_i^{l,0} - T_i^l(t))\,, \tag{8a}$$

$$q_i^l(t) = \theta_i^l(t)\, A_i^l \sqrt{p_i^s(t) - p_i^r(t)}\,, \tag{8b}$$

where $\theta_i^l \in [0, 1]$ is the load valve opening, and $f_c(\cdot)$ in (8a) represents a generic valve control law. Additionally, equation (8b) expresses the water flow model dependency on the pressure drop across the valve, and A_i^l is the fully open valve's section [39]. Note that the pressure drop across the load heat exchanger is not modeled as it is negligible compared to the pressure drop across pipes and control valves.

2) Thermal Generation Model: Each node $i \in \mathcal{G}$ absorbs a water flow $q_i^g \in \mathbb{R}_{\geq 0}$ at temperature T_i^r from the return distribution network and injects it into the supply network at temperature T_i^g, as in Figure 4(b). It holds that

$$P_i^g(t) = c\, q_i^g(t)\, (T_i^g(t) - T_i^r(t))\,, \quad \forall i \in \mathcal{G}\,, \tag{9}$$

where $P_i^g(t) \geq 0$ is the thermal power transferred by the generator to the absorbed water.

One of the generation nodes is denoted as "slack", and this is indicated with index $h \in \mathcal{G}$. The slack generator accomplishes two tasks: it imposes a reference pressure $p_h^{r,0}$ at the return network layer, thanks to a local expansion vessel, and maintains fixed pressure drop Δp_h^0 between supply and return, using a differential pressure pump [9], [42]. This implies that

$$p_h^s(t) = p_h^{r,0} + \Delta p_h^0\,, \qquad p_h^r(t) = p_h^{r,0}\,. \tag{10}$$

The slack node guarantees a minimum reference pressure in the water circuit and compensates for head losses [43]. Consequently, the slack node water flow cannot be externally imposed, as it is regulated locally to keep a constant pressure drop Δp_h^0. Differently, the other generation nodes can directly impose the water flow through local flow-regulated pumps. In particular, if Assumptions 1-4 hold, then the slack water flow entirely depends on the net water flow circulating in the DHN. In turn, the net flow is determined by the generators' flow-regulated pumps and by the load valve regulations. Finally, note that generation nodes can be either temperature-controlled, i.e., the output temperature T_i^g is externally imposed and tracked by a local controller, or power-controlled, i.e., a specific power P_i^g is requested to be delivered by the generator [8]. Thus, the generators' node set $\mathcal{G}$ includes the set of power-controlled nodes $\mathcal{G}_P$, and the set of temperature-controlled nodes $\mathcal{G}_T$, and it holds $\mathcal{G} = \mathcal{G}_P \cup \mathcal{G}_T$.

3) Storage Model: Thermal energy storage integration considerably increases DHN's flexibility [44]. TES connects the supply and return distribution networks and it can absorb/inject water from/to each network through a local pump, as illustrated in Figure 5.

Consider a generic thermal storage at node $i \in \mathcal{Z}$. Its total height is H_i^z, and its base radius is r_i^z. Concerning TES temperature dynamics, a one-dimensional stratified model is adopted. This modeling approach works similarly to the finite volume method used for pipes, as shown in Figure 5, [45]. Specifically, the storage tank is divided into n_i^z sections; each section has boundaries orthogonal to the water flow direction, height $h_i^z = H_i^z / n_i^z$ and volume $v_i^z = h_i^z \, \pi \, r_i^{z2}$.

Given that the thermal storage water flow, i.e., q_i^z, is bidirectional, as a convention, it is chosen that $q_i^z \geq 0$ when flowing from the return to the supply distribution network, and $q_i^z < 0$ when flowing in the opposite direction. Thus, for each storage section $k \in \{1, \dots, n_i^z\}$, the temperature model is defined as

$$\begin{aligned} c\rho v_i^z \, \dot{T}_{i,k}^z(t) = {} & 2\,\pi \, r_i^z \, h_i^z \, \alpha \, (T_i^{z,e}(t) - T_{i,k}^z(t)) \\ & + \pi \, r_i^{z2} \, \kappa \left((T_{i,k+1}^z(t) - T_{i,k}^z(t)) + (T_{i,k-1}^z(t) - T_{i,k}^z(t)) \right) \\ & + c \, q_i^z(t) \begin{cases} T_{i,k-1}^z(t) - T_{i,k}^z(t) & \text{if } q_i^z(t) \geq 0 \\ T_{i,k}^z(t) - T_{i,k+1}^z(t) & \text{if } q_i^z(t) < 0 \end{cases} \end{aligned} \tag{11}$$

where $T_{i,0}^z(t) = T_i^r(t)$ $T_{i,n_i^z+1}^z(t) = T_i^s(t)$ to express the interfacing of the storage tank with the supply and return network. The left-hand side of the above-equation expresses the thermal energy dynamics for the kth section, whereas the right-hand side considers the heat losses towards the external environment at temperature $T_i^{z,e}(t)$, the energy exchange with the adjacent sections due to thermal conduction, and the energy exchange due to mass transport phenomena, depending on the direction of the water flow.

Aiming to write thermal storage dynamics in a compact form, let us introduce the vector $\mathbf{T}_i^z(t) = \begin{bmatrix} T_{i,1}^z(t) & \dots & T_{i,n_i^z}^z(t) \end{bmatrix}'$ and consider again the matrices Φ and Ψ, and the vectors $\boldsymbol{\delta}$ and $\boldsymbol{\omega}$ defined in Section II-A. Thus, for each thermal storage node $i \in \mathcal{Z}$, the following temperature model holds

$$\begin{aligned} c \, \rho \, v_i^z \dot{\mathbf{T}}_i^z(t) = {} & 2\,\pi \, r_i^z \, h_i^z \alpha (\mathbb{1} \; T_i^{z,e}(t) - \mathbf{T}_i^z(t)) \\ & + \pi \, r_i^{z2} \, \kappa \, (\Psi + \Phi) \, \mathbf{T}_i^z(t) \\ & + c \, q_i^z(t) \begin{cases} \Phi \mathbf{T}_i^z(t) + \boldsymbol{\delta} T_i^r(t) & \text{if } q_i^z(t) \geq 0 \\ \boldsymbol{\omega} T_i^s(t) - \Psi \mathbf{T}_i^z(t) & \text{if } q_i^z(t) < 0 \end{cases} . \end{aligned} \tag{12}$$

C. Node Coupling Equations

Multiple water flows can converge or split in a single node, implying that node coupling equations must be introduced. Given a generic node $i \in \mathcal{N}$, we introduce the sets $\mathcal{I}_i^s \subset N$ and $\mathcal{I}_i^r \subset N$. These sets include the nodes delivering water to node i respectively at the supply and return distribution network and are defined as

$$\begin{aligned} \mathcal{I}_i^v(t) = {} & \{ j \in \mathcal{N} : (j,i) \in \mathcal{E} \wedge q_{ji}^v(t) \geq 0 \} \cup \\ & \{ j \in \mathcal{N} : (i,j) \in \mathcal{E} \wedge q_{ij}^v(t) < 0 \} , \end{aligned} \tag{13}$$

for $v \in \{s, r\}$. Note that the input node sets are time-varying, depending on the current direction of the water flow.

Thus, the overall water flow incoming at each node $i \in \mathcal{N}$ at the supply network is

$$q_i^s(t) = \sum_{\forall j \in \mathcal{I}_i^s(t)} (q_{ji}^s(t) - q_{ij}^s(t)) + \begin{cases} q_i^g(t) & \text{if } i \in \mathcal{G} \\ q_i^z(t) & \text{if } i \in \mathcal{Z} \wedge q_i^z(t) \geq 0, \end{cases} \tag{14a}$$

whereas the one on the return network is

$$q_i^r(t) = \sum_{\forall j \in \mathcal{I}_i^r(t)} (q_{ji}^r(t) - q_{ij}^r(t)) + \begin{cases} q_i^l(t) & \text{if } i \in \mathcal{L} \\ -q_i^z(t) & \text{if } i \in \mathcal{Z} \wedge q_i^z(t) < 0. \end{cases} \tag{14b}$$

Furthermore, the average temperatures at node i for the supply and return network are derived from the weighted average of the incoming water flow temperatures and their model are

$$\begin{aligned} q_i^s(t) T_i^s(t) = {} & \sum_{\forall j \in \mathcal{I}_i^s(t)} \left(q_{ji}^s(t) \, T_{ji,n_{ij}^s}^s(t) - q_{ij}^s(t) \, T_{ij,1}^s(t) \right) \\ & + \begin{cases} q_i^p(t) \, T_i^g(t) & \text{if } i \in \mathcal{G} \\ q_i^z(t) \, T_{i,n_i^z}^z(t) & \text{if } i \in \mathcal{Z} \wedge q_i^z(t) \geq 0, \end{cases} \end{aligned} \tag{15a}$$

and

$$\begin{aligned} q_i^r(t) T_i^r(t) = {} & \sum_{\forall j \in \mathcal{I}_i^r(t)} \left(q_{ji}^r(t) \, T_{ji,n_{ij}^r}^r(t) - q_{ij}^r(t) \, T_{ij,1}^r(t) \right) \\ & + \begin{cases} q_i^l(t) \, T_i^l(t) & \text{if } i \in \mathcal{L} \\ -q_i^z(t) \, T_{i,1}^z(t) & \text{if } i \in \mathcal{Z} \wedge q_i^z(t) < 0, \end{cases} \end{aligned} \tag{15b}$$

where the water temperature either at the first or last section is properly selected for pipes and storages based on the direction of the corresponding water flow.

Finally, considering the mass balance at each node $i \in \mathcal{N}$, the total incoming water flow is equal to the one outgoing from the node. Thus, introduce the set of output nodes $\mathcal{O}_i^s \subset \mathcal{N}$ and $\mathcal{O}_i^r \subset \mathcal{N}$ for the supply and return distribution network, respectively, which are defined as

$$\begin{aligned} \mathcal{O}_i^v(t) = {} & \{ j \in \mathcal{N} : (i,j) \in \mathcal{E} \wedge q_{ij}^v(t) \geq 0 \} \cup \\ & \{ j \in \mathcal{N} : (j,i) \in \mathcal{E} \wedge q_{ji}^v(t) < 0 \} , \end{aligned} \tag{16}$$

for $v \in \{s, r\}$. Thus, it holds that

$$q_i^s(t) = \sum_{\forall j \in \mathcal{O}_i^s(t)} (q_{ij}^s(t) - q_{ji}^s(t)) + \begin{cases} q_i^l(t) & \text{if } i \in \mathcal{L} \\ -q_i^z(t) & \text{if } i \in \mathcal{Z} \wedge q_i^z(t) < 0, \end{cases} \tag{17a}$$

and

$$q_i^r(t) = \sum_{\forall j \in \mathcal{O}_i^r(t)} (q_{ij}^r(t) - q_{ji}^r(t)) + \begin{cases} q_i^g(t) & \text{if } i \in \mathcal{G} \\ q_i^z(t) & \text{if } i \in \mathcal{Z} \wedge q_i^z(t) \geq 0. \end{cases} \tag{17b}$$

D. Simulation Environment and Library

The presented DHN model in (3)-(17) is exploited to build a simulation modeling library, named *DHN4Control* library, implemented in the Modelica environment, an object-oriented declarative language suitable for modeling of cyber-physical systems [46]. The developed *DHN4Control* library is available online on GitHub and free to be used [1].

The developed library proves to be flexible and computationally efficient when simulating large-scale DHN systems and it is particularly suited for applications where numerous subsequent simulations are necessary, e.g., during control tuning and testing. The library already includes various default parameters derived from tabulated data, which can be changed based on the user choices. Moreover, the components included in the *DHN4Control* library, whose models are described in previous sections, have been validated against their virtual counterparts from more complex modeling libraries, e.g., the ThermoPower library [14]. As discussed later in Section IV, the formulated DHN models are accurate while enabling the simulation of DHN systems in a shorter time and with fewer parameters with respect to standard simulation libraries, e.g., ThermoPower. The library implementation uses Modelica 4.0.0 on OpenModelica Editor 19.0 [47]. Thanks to Modelica and the OpenModelica environment, it is possible to create portable simulators using the FMU format. This format allows a wide range of software to run Modelica simulations. Among the supported software, but not restricted to, Matlab and Python. More details on these aspects are available in [1].

III. The Control Problem

In this section, a nonlinear model predictive control (NMPC) regulator is designed, capable of optimally coordinating DHN operations by minimizing operational costs while respecting all necessary constraints. This requires the development of an accurate dynamical system model efficiently solvable from the optimization perspective. In fact, despite the model assumptions introduced in Section II, the simulation-oriented DHN model could be still unpracticable for control purposes due to its dimension and complexity. Thus, model reduction procedures are here presented, enabling to obtain a control-oriented DHN model with enhanced computational efficiency and satisfactory modelling accuracy.

A. Control-Oriented Modelling

The NMPC control-oriented model derives from equations (3)-(17) by applying the following simplification steps.

1) Fixed Flow Direction in Distribution Pipes: Equations (3)-(5) have a switching characteristic related to the direction of the water flow. However, in practice, most supply and distribution network pipes have a fixed flow direction, which can be estimated either from operational data or through preprocessing techniques [9]. Because of this, we here assume that the flow direction in each pipe does not vary over time along the NMPC prediction horizon, avoiding implementing (4)-(5) as Mixed-Logic Dynamical (MLD) constraints [48]. This further implies that the input and output nodes in (14)-(17), i.e., $\mathcal{I}_i^v$ and $\mathcal{O}_i^v$ with $v \in \{s, r\}$, do not vary along the prediction horizon.

2) Storage Model Reformulation: Contrarily to distribution pipes, thermal storages require reversible flow for their operation as it is related to the charging/discharging modes (see equation (12)). Preserving the aim of mixed-integer variables avoidance in the NMPC problem, we reformulate the storage model similarly to typical battery models [49]. Hence, a charging water flow is introduced, i.e., $q_i^{z,s} \in \mathbb{R}_{\geq 0}$, identifying the water flow injected into the ith thermal storage from the supply distribution network (i.e., hot water), and a discharging water flow is introduced, i.e., $q_i^{z,r} \in \mathbb{R}_{\geq 0}$, identifying the one delivered to the supply network. Given that one single operating mode can be activated at each time instant, it must hold that

$$q_i^{z,s}(t) \cdot q_i^{z,r}(t) = 0. \tag{18}$$

Thus, the storage temperature model (12) is rewritten as

$$\begin{aligned} c\,\rho\, v_i^z \dot{\mathbf{T}}_i^z(t) = {} & 2\,\pi\, r_i^z\, h_i^z \alpha (\mathbb{1} T_i^{z,e}(t) - \mathbf{T}_i^z(t)) \\ & + \pi\, r_i^{z\,2}\, \kappa\, (\Psi + \Phi)\, \mathbf{T}_i^z(t) \\ & + c\, q_i^{z,s}(t)\, (\Phi\, \mathbf{T}_i^z(t) + \boldsymbol{\delta} T_i^r(t)) \\ & - c\, q_i^{z,r}(t)\, (\boldsymbol{\omega} T_i^s(t) - \Psi\, \mathbf{T}_i^z(t))\,, \end{aligned} \tag{19}$$

avoiding the explicit use of integer variables to activate the two different models. It is worth noting that one can adopt a similar reformulation for the models of distribution pipes in case the flow direction cannot assumed to be fixed along the prediction horizon.

3) Load Model Reduction and Pressure Modeling Removal: At the NMPC level, it is possible to assume that the load local control tracks the output load temperature reference, as discussed in [41], implying that

$$T_i^l(t) = T_i^{l,0}\,, \qquad \forall i \in \mathcal{L}. \tag{20}$$

Moreover, pressures are not directly related to the economic management of the DHN; consequently, we may exclude pressure equations from the NMPC problem formulation to reduce its dimension. Nevertheless, even though we neglect pressure equations, the water flows in distribution pipes must respect Kirchhoff's node and loop laws applied to hydraulics networks [50]. The former states that the ingoing and outgoing water flows at each node of $G = (\mathcal{N}, \mathcal{E})$ are balanced, which is guaranteed by (14) and (17). The latter states that the net pressure drop in each closed path of $G = (\mathcal{N}, \mathcal{E})$ must be null, both for the supply and the return distribution network. This property can be imposed without using pressure variables as described in the following.

Consider the DHN graph $G = (\mathcal{N}, \mathcal{E})$, and denote with m the number of its bounded faces, where a bounded face is a closed region of the plane fully delimited by edges and nodes [51]. Each kth graph face, with $k \in \{1, \ldots, m\}$, denotes an essential mesh of the graph, i.e., a mesh not containing any other mesh. Thus, denote with $\mathcal{M}_k \subseteq \mathcal{N}$ the set of nodes of each kth mesh and with $\gamma_k \subset \mathcal{M}_k \times \mathcal{M}_k$ a sequence of edges identifying a closed path visiting all nodes in $\mathcal{M}_k$. Moreover, for the sake of clarity, introduce $\zeta_{ij}^v = \text{sign}(q_{ij}^v(t))$, for each $(i, j) \in \gamma_k$ and $v \in \{s, r\}$, which is a fixed parameter being the water flow direction in pipes assumed to be constant. Hence, to impose that the net pressure drop is null for each closed

path, the following equations can be introduced for each kth mesh, with $k \in \{1, \dots, m\}$,

$$\sum_{\forall (i,j) \in \gamma_k} \zeta_{ij}^v \left(a_{ij}^s (q_{ij}^v(t))^2 + b_{ij}^v \right) = 0 \tag{21}$$

with $v \in \{s, r\}$, where a_{ij}^v, b_{ij}^v are defined as

$$a_{ij}^v = \begin{cases} \rho c_f \dfrac{L_{ij}^v}{r_{ij}^v} \dfrac{1}{(\rho \pi {r_{ij}^v}^2)^2} & \text{if } (i,j) \vee (j,i) \in \mathcal{E}_P, \\ \dfrac{k_{1,ij}^v \max(\zeta_{ij}^v, 0) + k_{2,ij}^v \min(\zeta_{ij}^v, 0)}{2\rho} & \text{if } (i,j) \vee (j,i) \in \mathcal{E}_F, \end{cases} \tag{22}$$

$$b_{ij}^v = \begin{cases} g y_{ij}^v & \text{if } (i,j) \vee (j,i) \in \mathcal{E}_P, \\ 0 & \text{if } (i,j) \vee (j,i) \in \mathcal{E}_F, \end{cases} \tag{23}$$

for each $(i, j) \in \gamma_k$. As evident, (21) exploits (4) and (5) to impose an overall null pressure drop at each kth mesh, without using pressure variables and with a lower number of equations (two equations for each mesh, one for the supply and one for the return network, instead of two equations for each edge).

Now, consider the original DHN model (3)-(17) and note that pressure variables p_i^s, p_i^r and the load valve opening θ_i^l appear solely in (4), (5), (8), (10). If these variables and equations are excluded from the NMPC control-oriented model, whereas (20) and (21) are added, the number of removed equations from the original DHN model is $n_{re} = 2|\mathcal{E}| + 2 + |\mathcal{L}| - 2m$, whereas the net number of removed variables is $n_{rv} = 2|\mathcal{N}| + |\mathcal{L}|$. To ensure that the remaining DHN model is still properly formulated, the number of removed equations and variables must match. This is proved to be true due to Euler's formula in graph theory [51], stating that the number of bounded graph faces is always

$$m = |\mathcal{E}| - |\mathcal{N}| + 1 \ , \tag{24}$$

which, in turns, implies that $n_{re} = n_{rv}$. Note that in case a radial DHN graph is considered, i.e., $m = 0$, equations (21) are not introduced, and the variables p_i^s, p_i^r, and θ_i^l and equations (4), (5), (8), (10) can be removed from the overall model by simply adding (20).

4) Distribution Pipes Temperature Model Reduction: Distribution pipe modeling involves separate models for the water and pipe wall temperature dynamics (3). Nevertheless, at the NMPC level, a reasonable modeling reduction is adopted, describing the overall energy exchange in each finite-volume section of distribution pipes.

First of all, consider the pipe wall temperature model (3b) which can be rewritten as

$$\dot{\mathbf{T}}_{ij}^{vm}(t) = \frac{2\pi l_{ij}^v U_{ij}^m}{c_m \rho_m v_{ij}^{vm}} \left(r_{ij}^v \left(\mathbf{T}_{ij}^v(t) - \mathbf{T}_{ij}^{vm}(t) \right) - \frac{U_{ij}^e}{U_{ij}^m} r_{ij}^{vm} \left(\mathbf{T}_{ij}^{vm}(t) - \mathbb{1} T_{ij}^{v,e}(t) \right) \right), \tag{25}$$

for $v \in \{s, r\}$. Considering that pipes are usually insulated and that the heat transfer coefficient between water and the pipe wall is typically high, it follows that $\frac{U_{ij}^e}{U_{ij}^m} \ll 1$ (for the case study in Section IV, $\frac{U_{ij}^e}{U_{ij}^m} \simeq 10^{-5}$ $\forall$ $(i, j) \in \mathcal{E}$). Hence, the pipe wall temperature model can be approximated as

$$\dot{\mathbf{T}}_{ij}^{vm}(t) = \frac{2\pi r_{ij}^v l_{ij}^v U_{ij}^m}{c_m \rho_m v_{ij}^{vm}} \left(\mathbf{T}_{ij}^v(t) - \mathbf{T}_{ij}^{vm}(t) \right), \tag{26}$$

for $v \in \{s, r\}$. Now, note that the pipe wall thermal dynamic time constant $\tau_{ij}^{vm} = (c_m \rho_m v_{ij}^{vm})/(2\pi r_{ij}^v l_{ij}^v U_{ij}^m)$ is usually relatively small compared to the DHN thermal dynamics (for the case-study in Section IV, $\tau_{ij}^{vm} \simeq 10$s). Therefore, as the usual NMPC sampling time is $\tau_s \gg \tau_{ij}^{vm}$, we can assume that the pipe wall and the water are always at thermal equilibrium, i.e., $\mathbf{T}_{ij}^v(t) = \mathbf{T}_{ij}^{vm}(t)$, at least at the NMPC level. For notational simplicity, the variable $\mathbf{T}_{ij}^v(t)$ will describe the overall temperature of the corresponding distribution pipe, with $v \in \{s, r\}$.

Thus, in the NMPC problem formulation, we substitute the distribution pipe temperature model (3) with the following

$$\begin{aligned} (c\rho v_{ij}^v + c_m \rho_m v_{ij}^{vm}) \dot{\mathbf{T}}_{ij}^v(t) = & c\, q_{ij}^v(t) \left(\Phi \mathbf{T}_{ij}^v(t) + \delta T_i^v(t) \right) \\ & - 2\pi r_{ij}^{vm} l_{ij}^v U_e \left(\mathbf{T}_{ij}^v(t) - \mathbb{1} T_{ij}^{v,e}(t) \right), \end{aligned} \tag{27}$$

for $v \in \{s, r\}$, where the left-hand side describes the stored thermal energy in each pipe section, comprising the pipe wall and water; whereas the right-hand side includes the energy exchanged due to transport phenomena and the heat losses towards the ambient. Note that (27) can be directly obtained by summing (3a) and (3b), assuming the water and pipe wall temperature at equilibrium as described.

It is worth noting that the proposed simplification allows to remove the following number of variables and equations

$$n_r = \sum_{\forall (i,j) \in \mathcal{E}_P} (n_{ij}^s + n_{ij}^r), \tag{28}$$

from the original DHN model (3)-(17), significantly contributing to the reduction of the NMPC problem complexity.

Remark 1: The number of sections in pipes and thermal storages is also a tunable parameter, as they can be reduced in the NMPC model based on the desired computational complexity and modeling accuracy.

In conclusion, the reduced DHN control-oriented model for the NMPC design is constituted by (6), (7), (9), (14)-(27). Collecting the states variables in the vector x, the input variables in the vector u, the exogenous signals in d, i.e.,

$$x = [\, (\mathbf{T}_{ij}^{s\prime}, \mathbf{T}_{ij}^{r\prime})_{ij \in \mathcal{E}_\mathcal{P}}, \mathbf{T}_{i \in \mathcal{Z}}^{z\prime} \,]', \tag{29a}$$

$$u = [\, T_{i \in \mathcal{G}_T}^g, P_{i \in \mathcal{G}_P}^g, q_{i \in \mathcal{G} \setminus h}^g, (q_i^{z,s}, q_i^{z,r})_{i \in \mathcal{Z}} \,]', \tag{29b}$$

$$d = [\, (P_i^l, T_i^{l,0})_{i \in \mathcal{L}}, T_{i \in \mathcal{Z}}^{z,e}, T_{ij \in \mathcal{E}}^{s,e}, T_{ij \in \mathcal{E}}^{r,e} \,]', \tag{29c}$$

and the remaining auxiliary variables of the model in the vector w, i.e.,

$$w = [\, (T_i^s, T_i^r)_{i \in \mathcal{N}}, (q_i^l, T_i^l)_{i \in \mathcal{L}}, (q_{ij}^s, q_{ij}^r)_{ij \in \mathcal{E}}, T_{i \in \mathcal{G}_P}^g, P_{i \in \mathcal{G}_T}^g, q_h^g \,]'. \tag{29d}$$

It follows that (19) and (27) can be rewritten compactly

$$\dot{x}(t) = f(x(t), u(t), d(t), w(t)) \,, \tag{29e}$$

whereas (6), (7), (9), (14)-(18), (20)-(21) as

$$g(x(t), u(t), d(t), w(t)) = 0\,, \tag{29f}$$

where $f(\cdot)$ and $g(\cdot)$ are suitable defined nonlinear functions.

B. NMPC Optimization Problem

The DHN control-oriented model (29) formulation uses discrete time with a sampling time τ_s for the design of the NMPC regulator. We introduce the discrete time index $k_s \in \mathbb{N}$ that defines the time instant $t = \tau_s k_s$ when the NMPC is executed. Therefore, denoting with $k \in \{k_s, \ldots, k_s + N_s - 1\}$ the generic time index along the prediction horizon, with N_s indicating the number of prediction steps, the DHN control-oriented model (29) is formulated in discrete-time as

$$x(k+1) = \tilde{f}(x(k), u(k), d(k), w(k))\,, \tag{30a}$$
$$g(x(k), u(k), d(k), w(k)) = 0\,. \tag{30b}$$

In (30a), $\tilde{f}(\cdot)$ derives from $f(\cdot)$ applying a suitable integration method. The control variables are constrained within their physical limits as

$$\underline{u} \le u(k) \le \bar{u}\,, \tag{31}$$

whereas state and auxiliary variables are bounded using soft constraints, i.e.,

$$\underline{x} - \sigma_x(k) \le x(k) \le \bar{x} + \sigma_x(k)\,, \tag{32}$$
$$\underline{w} - \sigma_w(k) \le w(k) \le \bar{w} + \sigma_w(k)\,, \tag{33}$$

where σ_x and σ_w are slack variables such that

$$\sigma_x(k) \ge 0, \quad \sigma_w(k) \ge 0\,. \tag{34}$$

At this stage, an additional auxiliary variable is introduced, defined as a function of the state variables, i.e., $e = \xi(x(k_s)) \in \mathbb{R}_{\ge 0}$. This variable expresses the total thermal energy stored in the DHN plant when the NMPC is executed and is defined as

$$\begin{aligned} e(k_s) = \xi(x(k_s)) = & \sum_{(i,j)\in\mathcal{E}_P} (c\rho v_{ij}^s + c_m \rho_m v_{ij}^{sm})\, \mathbb{1}'\, \mathbf{T}_{ij}^s(k_s) \\ & + \sum_{(i,j)\in\mathcal{E}_P} (c\rho v_{ij}^r + c_m \rho_m v_{ij}^{rm})\, \mathbb{1}'\, \mathbf{T}_{ij}^r(k_s) \\ & + \sum_{i\in\mathcal{Z}} c\,\rho\, v_i^z\, \mathbb{1}'\, \mathbf{T}_i^z(k_s)\,, \end{aligned} \tag{35}$$

where the total thermal energy contained in each water pipe and storage is included. Considering that the NMPC regulator is executed with a prediction horizon of N_s steps, the stored thermal energy of the following constraint is stated

$$e^0 - \sigma_e \le e(k_s + N_s) \le e^0 + \sigma_e\,, \tag{36}$$

with e^0 is a nominal thermal energy reference, and σ_e a slack variable such that

$$\sigma_e \ge 0\,. \tag{37}$$

The idea of (36) is to act as a terminal constraint, imposed as soft for the sake of feasibility so that the NMPC manages the DHN at minimum cost without fully discharging the thermal energy in storages and pipes [52]. The nominal energy reference can be computed using the nominal state values x^0, e.g., $e^0 = \xi(x^0)$. Hence, denoting the vector of slack variables as $\sigma = [\sigma_x', \sigma_w', \sigma_e]'$, the designed NMPC cost function is

$$\begin{aligned} J(k) = & \sum_{i\in\mathcal{G}} \left(c_i^g(k) \frac{P_i^g(k)}{\eta_i^g} + \eta_i^q c_i^q(k) q_i^g(k) \right) \\ & + \sum_{i\in\mathcal{Z}} \eta_i^z c_i^z(k) \left(q_i^{z,s}(k) + q_i^{z,r}(k) \right) + c_\sigma' \sigma(k)\,. \end{aligned} \tag{38}$$

In (38), the main goal is to minimize production costs in generators, considering the efficiency from primary to thermal energy η_i^g and the primary energy cost c_i^g (e.g., in the case of a heat pump, η_i^g would be the pump's coefficient of performance and c_i^g the electrical energy price). The electric consumption of generation pumps is also minimized, modeling it as proportional to the water flow q_i^g through a constant efficiency η_i^q [8]. The same idea applies to thermal storage pumps, recalling that $q_i^{z,s}$ and $q_i^{z,r}$ are not simultaneously different from zero. Finally, slack variables are penalized in (38) through the vector cost c_σ, commonly selected as much higher than the other costs to ensure constraints satisfaction.

Thus, the NMPC problem, solved at each $t = \tau_s k_s$, is

$$\min_{u(\cdot),\,\sigma(\cdot)} \quad \sum_{k=k_s}^{k_s+N_s-1} J(k) \tag{39a}$$
$$\text{subject to} \quad (30) - (37),\ \forall k \in \{k_s, \ldots, k_s + N_s - 1\}, \tag{39b}$$
$$x(k_s) = \tilde{x}_0\,, \tag{39c}$$

where $\tilde{x}_0$ corresponds to the current system state.

Remark 2: It is worth noting that, by adding suitable constraints and cost terms, more advanced energy management strategies can be included in (39), e.g., considering the energy trading with the electrical grid or minimizing the CO_2 emissions in case fossil and renewable primary sources are exploited to generate thermal power [8], [23].

1) State Estimation: It is paramount to consider the availability of state variables, given (39c), as not all of them could be measurable in a typical DHN plant. An example of non-measurable state variables is the temperatures of internal sections of pipes, where sensors are typically not placed. Thus, the use of state observers may be necessary. In this context, one effective solution is to employ an Extended Kalman Filter as this is capable of estimating the overall state x by exploiting the knowledge of the input u in (29b), of the DHN model (29), and of an output vector $y = [\,(T_i^s\,, T_i^r)_{\forall i\in\mathcal{N}}\,]$, which can be assumed measurable, since each node $i \in \mathcal{N}$ is a significant DHN component (e.g., a generator, a load, or a thermal storage). The formulation of the implemented Extended Kalman Filter is not reported as this is standard, and the reader can refer to [53] for further details.

IV. Case Studies

In this section, we first describe the Thermal Test Facility. It is a district heating network currently under construction at the research center Ricerca sul Sistema Energetico - RSE S.p.A., Milan. Thanks to the Thermal Test Facility, the simulation model, presented in Section II, as well as the control-oriented model, introduced in Section III, can benefit

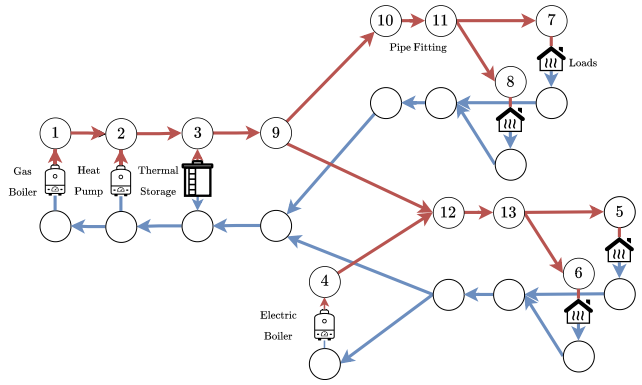

Fig. 6. Schematic of the DHN Thermal Test Facility located at Ricerca sul Sistema Energetico - RSE S.p.A.

from real-world data to guarantee meaningful outputs. Secondly, the dynamic simulation library and the control-oriented model are validated using experimental data and other simulation libraries. After successful validation, the two models are implemented to test and derive the NMPC regulator, presented in Section III, considering 24h of DHN operations. All test scenarios run on a laptop with processor Intel(R) Core(TM) i7-6700HQ CPU @ 2.60GHz, RAM 16.0 GB.

A. Case Study 1: The Thermal Test Facility

The Thermal Test Facility of RSE, when finished, will be an experimental benchmark emulating a real DHN plant and its joint operation with other forms of energy, i.e., hydrogen, natural gas, and electricity. The DHN system, reported in Figure 6, consists of 13 nodes and 2 parallel branches. The main parameters of the Thermal Test Facility are reported in Table II. Being a multi-producer DHN, it comprises 3 thermal generators, i.e., a gas boiler (node 1), a heat pump (node 2), and an electric boiler (node 4). Moreover, the DHN case study features a thermal energy storage unit (node 3) and four thermal loads (nodes 5, 6, 7, 8). Pipes connecting loads to the DHN main pipeline are thinner, implying that pipe fittings are introduced in the edges $(10, 11)$ and $(12, 13)$. The gas boiler at node 1 is temperature-controlled, and it operates as a slack generation node (i.e., $h = 1$), imposing a pressure reference $p_1^{r,0} = 2.5$ bar at the return network and a pressure increase at the supply network equal to $\Delta p_1^0 = 2.5$ bar through the local pump, as discussed in Section II-B2. On the other hand, the heat pump at node 2 and the electric boiler at node 4 are power-controlled and equipped with local pumps regulated to deliver a fixed water flowrate of 0.5 and 0.8 [kg/s] for the electric boiler and the heat-pump respectively.

In the same way, the thermal energy storage pump is flow-controlled and has a maximum water mass flow of 0.5 kg/s, whereas the TES total volume of 11.35 m^3.

Finally, loads satisfy their thermal demand by absorbing a water flow from the DHN supply network. The flow absorption is regulated to track a return temperature of $T_i^{l,0} = 65$°C through a PI controller. This control acts on an electric valve with a maximum opening area of 67 cm^2. Finally, the supply temperature must be higher than 75°C to ensure the proper functioning of the load heat exchangers.

TABLE II
MAIN PARAMETERS OF THE THERMAL TEST FACILITY AT RICERCA SUL SISTEMA ENERGETICO - RSE S.P.A

Pipes $(i,j) \in \mathcal{E}_P$	L_{ij}^v [m]	r_{ij}^v [cm]	r_{ij}^{vm} [cm]
$(1,2)$	4.5	2.54	2.94
$(2,3)$	1	2.54	2.94
$(3,9)$	17.5	2.54	2.94
$(4,12)$	35	2.54	2.94
$(9,10)$	2.25	2.54	2.94
$(9,12)$	1.51	2.54	2.94
$(11,7)$	8	1.27	2.94
$(11,8)$	15	1.27	2.94
$(13,5)$	13	1.27	2.94
$(13,6)$	10.75	1.27	2.94
Generators $i \in \mathcal{G}$	$(\underline{P}_i^g, \bar{P}_i^g)$ [kW]	$(\underline{T}_i^g, \bar{T}_i^g)$ [°C]	η_i^g [-]
1	$(0, 120)$	$(75, 85)$	0.84
2	$(0, 11)$	$(65, 90)$	5
4	$(0, 50)$	$(65, 90)$	0.92
TES $i \in \mathcal{Z}$	H_i^z [m]	A_i^z [m^2]	$(\alpha,\ \kappa)$ [W/K·m^2]
3	5	2.27	$(6.89, 1.62e^{-4})$

1) Model Validation: The simulation and the control-oriented models, respectively introduced in Section II and III, are hereafter validated before, being exploited for testing the designed control strategy.

a) Simulator model validation: The *DHN4Control* library, exploiting the DHN simulation model, is validated against an existing library, i.e., *ThermoPower* [14]. ThermoPower is a suitable choice as it includes one-dimensional finite-volume pipes with metal wall inertia models similar to those proposed in this paper. We compare the two libraries using real-world experimental data of a 39 m water pipe [54]. The simulated pipes use $n = 25$ sections. The validation test compares the water temperature at the pipe outlets given the same initial conditions, as shown in Figure 7 having on y axis the temperature and on the x axis the time. In particular, the *DHN4Control* library seems accurate, as it matches the experimental data and ThermoPower's output. We employ the root mean square error (RMSE) as the performance index and observe that ThermoPower achieves an RMSE of 0.74, whereas the DHN4Control reaches 0.82. On the other hand, the main difference between the two simulation libraries is computational time. Considering the discussed test, ThermoPower simulation required 3.47 s; in comparison, the *DHN4Control* library required only 0.03 s. In fact, given the different involved pipe models, the simulator implemented with *DHN4Control* has 179 variables and equations, whereas the ThermoPower simulator has up to 1255 variables and equations. The difference is because the *ThermoPower* model is considerably more complex compared to the one described in Section II, as it accounts for other physical phenomena that are not of interest for DHNs and, especially, for their control testing, e.g., fluid phase-changing or compressibility. Note that the described results are satisfactory even though the experimental data used to validate the models are in

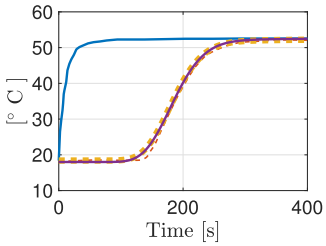

Fig. 7. Validation of the pipe model in [54]. Temperature of the water fed to the pipe (solid blue line). Water temperatures measured at the end of the pipe: (i) experimental (dashed red line), (ii) ThermoPower simulation (solid purple line), (iii) DHN4Control simulation (yellow dotted line).

the temperature range 18-55 °C, which is outside the one considered in the *DHN4Control* library, where the values of ρ, c reported in Assumption 1 are computed.

b) Control-oriented model validation: The control-oriented model derived in Section III is validated against the *DHN4Control* library. Specifically, a 24-hour scenario is considered for both the simulation (3)-(17) and the control-oriented (30) models, the latter using a sampling time of $\tau_s =$ 1800 s. The control-oriented model considers two sections for each pipe, whereas, in the simulation model, the pipes' section number vary between 2 to 10 depending on the pipe's length. Regarding the TES, given its reduced dimension, 2 sections are used both for the simulation and the control-oriented model. The control-oriented model has 50 optimization variables for each time step; whereas, the simulation model has 471 variables. To evaluate models performance, the DHN simulation and the control-oriented models are fed with the same known inputs, which are reported in Figure 8. These are: the gas boiler temperature reference (Figure 8(a)), the loads thermal demand (Figure 8(b)), the electric boiler power reference (Figure 8(c)), and the TES mass flow (Figure 8(d)). Figure 9 shows the obtained results for the DHN simulation and the control-oriented model. As shown in Figure 9(a), the thermal energy storage layers' temperature transients almost coincide with the simulated ones. The same holds for the supply temperature at the furthest thermal load, which profile is almost equivalent for the simulation and control-oriented model, as shown in Figure 9(b). To conclude, although pressure variables do not appear in the control-oriented model, the DHN water flow almost coincides for the simulated and control-oriented model, as reported in Figure 9(c).

2) Optimal Control Results: In this section, we present the NMPC design. The NMPC optimization problem uses the environment CasADi in MATLAB for the implementation of the optimization problem [55] and Ipopt as solver [56]. The NMPC is designed with a prediction horizon of $12h$ and a sample time of $\tau_s = 1800s$ for a total of $N_s = 12/\tau_s = 24$ steps. Since the MPC requires state measurements, an Extended Kalman Filter is implemented as described in Section III-B1. To test the designed NMPC regulator, it runs for 24 hours, employing the thermal demand profile depicted in Figure 8(a) for each thermal load. Moreover, time-varying costs for the primary energy sources are considered, i.e., for gas and electricity, and these are depicted in Figure 10(a).

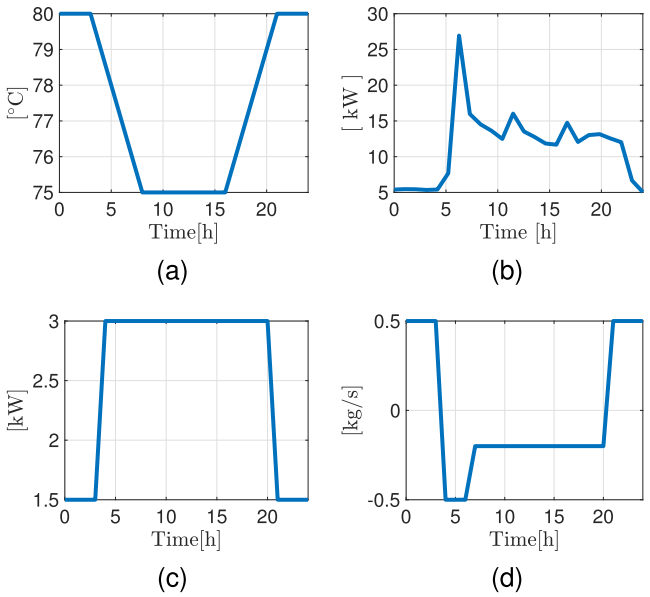

Fig. 8. Inputs and disturbances used for the simulation and control-oriented model comparison: (a) Gas boiler output temperature. (b) Thermal demand of each load. (c) Electric boiler power input. (d) Thermal storage water flow.

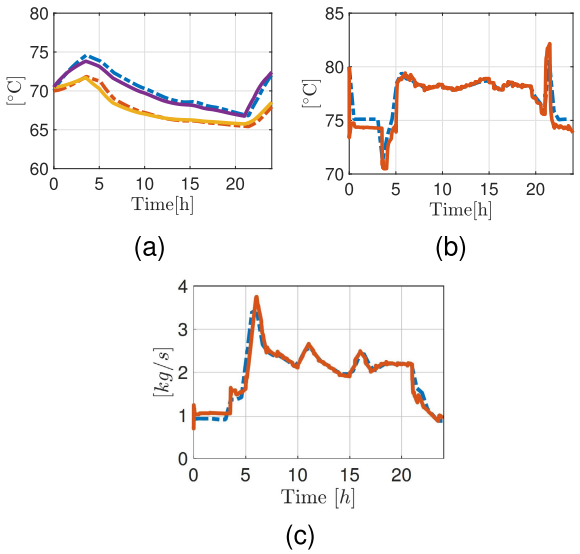

Fig. 9. DHN simulation (solid lines) and control-oriented model (dashed lines) comparison: (a) TES temperatures at layer 2, i.e., the top layer, (solid purple and dashed blue) and at layer 1, i.e., the bottom one, (solid yellow and dashed orange); (b) Load 3 supply temperature; (c) Water flow at the slack generator.

Figures 10(b)-(h) report the results of the NMPC regulation applied to a 24 hours scenario. Hereafter, we analyze the results. Given the high cost of gas compared to electricity, the NMPC never uses the gas boiler (node 1) at its maximum power, i.e., $\bar{P}_1 = 120$ kW, as depicted in Figure 10(b). Instead, the heat pump (node 2) runs at max capacity due to its high efficiency, except at night when thermal loads require less power, see Figure 10(c). Additionally, the electric boiler (node 4) turns on only when convenient, e.g., its power generation significantly decreases when the electricity cost reaches peak prices, i.e., at 8:00 and 20:00, as shown in Figure 10(d).

Furthermore, the NMPC exploits the thermal storage to reduce operational costs. As the heat pump is the most

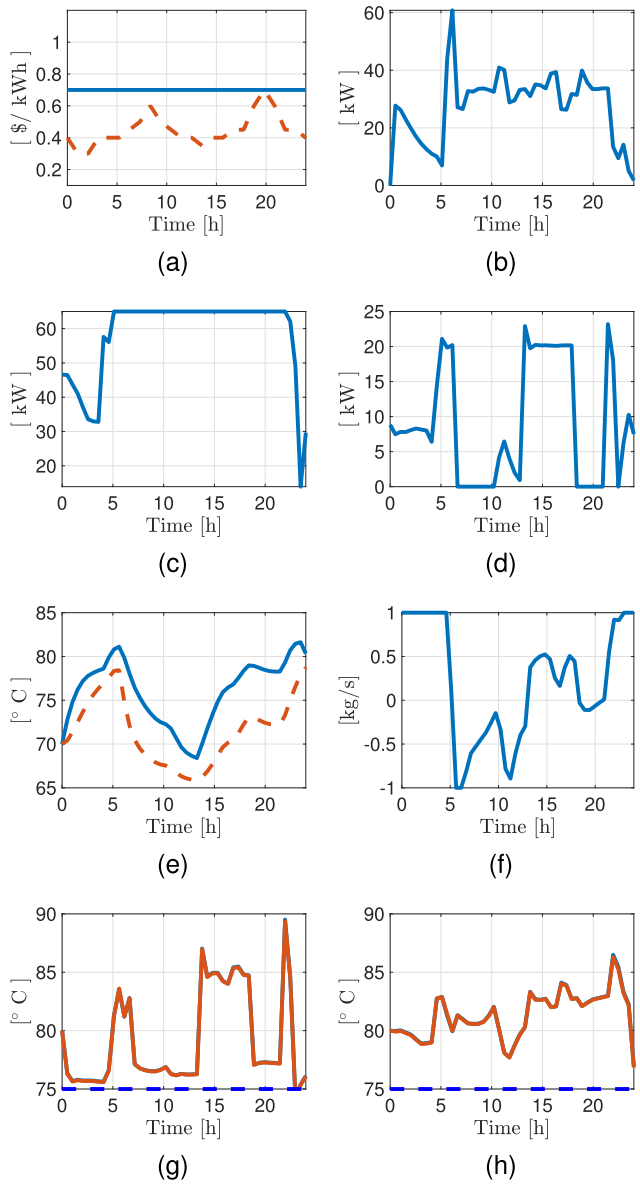

Fig. 10. Case study results: (a) Energy costs: gas (solid line) and electricity (dashed line). (b) Gas boiler power. (c) Heat pump power. (d) Electric boiler power. (e) TES Layers' temperature (solid line - hot layer, dashed line - cold layer). (f) TES Mass flow. (g) Load supply temperature at nodes 7, 8. (h) Load supply temperature at nodes 5, 6.

convenient component of the network and is saturated almost all day, the TES is precharged during the night, also considering that the electrical price is lower. Then, when thermal load demand peaks (i.e., around 6:00, as depicted in Figure 8(d)), the TES delivers hot water to the supply network. Another shorter cycle of charge/discharge happens in the afternoon, 14:00 - 21:00. Please refer to Figure 10(e) to visualize the temperatures of the TES sections, and to Figure 10(f) for the TES water flow.

Altogether, the joint effects of the generators and TES can be appreciated from 14:00 to 18:00. In this time frame, the electricity energy cost and the thermal demand are lower. Therefore, the TES absorbs hot water from the supply, thus charging. However, the heat pump can divert little energy into the storage, as it already runs at max power output. Therefore, the NMPC, to redirect more energy from the heat pump to the storage, turns the electric boiler on to supply loads 5 and 6, being the closest generator.

TABLE III
TOTAL VALUES OF THERMAL POWER GENERATION AND COSTS FOR THE RULE-BASED SIMULATION AGAINST THE NMPC CONTROL

Control	Generated energy	Operating cost
Test Facility Rule Based	1959.5 kWh	898.3 $
Test Facility NMPC	1690.6 kWh (-14%)	763.2 $ (-15%)
AROMA Rule Based	4494.7 kWh	2100.6 $
AROMA NMPC	4183.7 kWh (-7%)	1897.4 $ (-10%)

Moreover, because of the inclusion of DHN thermal dynamics, the NMPC can pre-charge pipes with hot water when convenient or before load peaks, a strategy known as packing and depicted in Figure 10(g) and (h). The pipe packing starts at 5:00, while the peak of consumption happens at around 6:00. Another effect of including DHN thermal dynamics in the NMPC formulation is the ability to operate the system at the lower supply temperature when the energy costs are higher without violating the constraints on the minimum supply temperature for loads, i.e. 75°C, as illustrated in Figure 10(g)-(h).

The NMPC performances are compared with a rule-based control strategy, similar to the ones applied in real DHNs [8]. The rule-based strategy is simple: *(i)* the gas boiler reference temperature is constant during the day, and between 22:00 and 5:00, it turns off, given lower thermal demand; *(ii)* the electric boiler runs at a fixed power production all day, while the heat pump runs at max power during the day and less during the night, between 22:00 to 5:00; *(iii)* the TES is operated with the same profile of the NMPC optimal management.

For a 24*h* simulation, the obtained results are shown in Table III where it is evident that the management cost of the rule-based strategy is higher than the NMPC one, achieving a net saving of roughly 15%. The total thermal energy produced by the NMPC is also lower because of the optimizer's ability to operate the DHN more efficiently, satisfying network constraints with lower temperatures. Finally, it is worth noting that despite a prediction horizon of 12 hours and considered a nonlinear model, the average NMPC computational time is 5s, mainly due to the control-oriented modeling approach presented in Section III. To better assess the computational performances achieved by the control-oriented model, a NMPC regulator including the DHN simulation model, i.e., the one described in Section II, has been also developed for the RSE Test Facility, maintaining the same cost function, prediction horizon and constraints. It resulted that the computational time becomes on average 1000s, which is much higher with respect to the one achieved with the control-oriented model, witnessing the benefits of the proposed approach. It is worth noting that the computational time of a controller introduces a delay in the control loop, which, if large, can significantly affect control performances and stability.

B. Case Study 2: AROMA Network

The proposed methods are tested in a second case-study, i.e., the AROMA district heating network [9]. The AROMA DHN is a meshed network comprising more than 7 km of

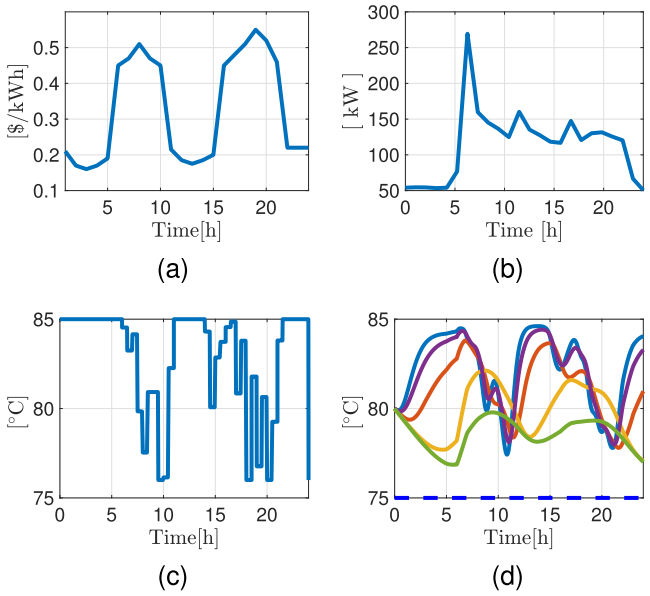

Fig. 11. NMPC results for case-study 2: (a) Electrical Energy prices. (b) Thermal load profile. (c) Generator supply temperature. (d) loads' supply temperatures (dashed line indicating lower bound).

pipelines (roughly 20 times larger than the RSE Test Facility), a total of 24 nodes (considering also pipe fitting nodes), a temperature-controlled generator, and five thermal loads. The AROMA network simulation model, defined according to Section II, involves 882 variables for each time step. After the implementation of the model reduction steps described in Section III-A, the control-oriented model consists of just 86 variables per time step. The NMPC regulator is designed considering a sampling time of 30 minutes and a prediction horizon of 48 steps, i.e., 24h. Also in this case study, the supply temperature of loads is constrained to exceed a lower bound of 75°C. Moreover, the energy prices and the thermal load profiles are reported in Figure 11(a) and (b), respectively. The obtained control results are reported in Figure 11(c) and (d). In particular, during low-price time periods (22:00-6:00, 12:00-16:00), the NMPC increases the temperature in the supply pipelines, acting on the thermal generator. On the opposite, during price peaks the generator temperature is reduced, as evident from Figure 11(c), and the stored thermal energy in pipelines is exploited to satisfy the thermal demand. Moreover, the supply temperature at loads is always maintained higher than 75°C, as required by operational constraints. Given the computational-efficiency of the control-oriented model, the designed NMPC regulator requires on average 30 seconds to compute its optimal control action. Finally, the performances of the designed NMPC regulator is compared against a rule base-strategy, operating the thermal generator at a constant supply temperature, as done in Section IV-A. The results are reported in Table III, showing that the achieved cost savings are approximately 10%. Note that, differently from the RSE Test Facility described in Section IV-A, here a thermal storage is not available, meaning that just the network thermal inertia is exploited to decrease the costs.

V. Conclusion

In this article, we presented the development of a simulation and a control-oriented district heating network (DHN) model, together with the design of a nonlinear predictive control (NMPC) regulator able to achieve significant energy savings with respect to a rule based strategy. The simulation model performed accurately and efficiently because of carefully chosen assumptions; its implementation led to the development of the *DHN4Control* library, freely available online [1]. Additionally, we proposed a control-oriented optimization model, particularly efficient due to a model reduction procedure. Finally, these two models were validated against experimental and virtual data, showing high accuracy performances despite their reduced complexity. Moreover, the designed NMPC regulator achieves a significant cost reduction (up to 18%) with respect to a benchmark rule-based control strategy, with reduced computational times. The reduction is possible thanks to the control-oriented model capable of leveraging the DHN thermal inertia, i.e., in storages and pipes, minimizing costs, energy production, and satisfying operative constraints over the whole network. The proposed methodology can be also exploited for thermo-hydraulic applications other than DHN systems, e.g., for cooling systems for industrial processes or for building heating systems. In fact, also in these case, a reduced control-oriented model can be crucial for the design of cost-effective and computationally-efficient NMPC regulators maximizing energy efficiency. Future work will consider introducing new components for the DHN, which would lead to the investigation of innovative energy management control strategies. Moreover, more structured DHN frameworks can be taken into account, considering the presence of independent energy hubs and prosumers optimally regulating their thermal power exchange with the DHN system. In this context, future research directions may focus on the design of distributed NMPC architectures, each one regulating a sub-network or an aggregation of thermal prosumers, so as to optimize their internal operation and thermal power exchanges over the DHN. Finally, a further future development will consist in the implementation of the proposed control solution to the real Thermal Test Facility in RSE - Ricerca sul Sistema Energetico S.p.A., as it will be soon available for testing, so as to experimentally assess the achievable performances.

Acknowledgment

The work of Alessio La Bella and Riccardo Scattolini was carried out within the MICS (Made in Italy - Circular and Sustainable) Extended Partnership and received funding from Next-Generation European Union (EU) (Italian Piano Nazionale di Ripresa e Resilienza (PNRR) - M4 C2, Invest 1.3 - D.D. 1551.11-10-2022, PE00000004). CUP MICS D43C22003120001.

References

[1] L. Nigro. (2023). *DHN4Control: A Modelica Library for Hydro-Thermal Simulations District Heating System*. [Online]. Available: Https://github.com/Lollo-sk/DHN4Control

[2] T. Goodson. (2022). *Heating*. [Online]. Available: https://www.iea.org/reports/heating

[3] E. Commission. (2016). *Communication From the Commission to the European Parliament, the Council, the European Economic and Social Committee and the Committee of the Regions an Eu Strategy on Heating and Cooling*. [Online]. Available: https://eurlex.europa.eu/legal-

[4] B. Rezaie and M. A. Rosen, "District heating and cooling: Review of technology and potential enhancements," *Appl. Energy*, vol. 93, pp. 2–10, May 2012.

[5] S. Paardekooper et al. (2018). *Heat Roadmap Europe 4: Quantifying the Impact of Low-Carbon Heating and Cooling Roadmaps*. [Online]. Available: https://vbn.aau.dk/en/publications/heat-roadmap-europe-4-quantifying-the-impact-of-low-carbon-heatin

[6] S. Werner, "Network configurations for implemented low-temperature district heating," *Energy*, vol. 254, Sep. 2022, Art. no. 124091.

[7] S. Buffa, M. H. Fouladfar, G. Franchini, I. L. Gabarre, and M. A. Chicote, "Advanced control and fault detection strategies for district heating and cooling systems—A review," *Appl. Sci.*, vol. 11, no. 1, p. 455, Jan. 2021.

[8] A. La Bella and A. Del Corno, "Optimal management and data-based predictive control of district heating systems: The novate milanese experimental case-study," *Control Eng. Pract.*, vol. 132, Mar. 2023, Art. no. 105429.

[9] R. Krug, V. Mehrmann, and M. Schmidt, "Nonlinear optimization of district heating networks," *Optim. Eng.*, vol. 22, no. 2, pp. 783–819, Jun. 2021.

[10] S.-A. Hauschild et al., "Port-Hamiltonian modeling of district heating networks," in *Progress in Differential-Algebraic Equations II*. Cham, Switzerland: Springer, 2020, pp. 333–355.

[11] J. E. Machado, M. Cucuzzella, and J. M. A. Scherpen, "Modeling and passivity properties of multi-producer district heating systems," *Automatica*, vol. 142, Aug. 2022, Art. no. 110397.

[12] F. Strehle, J. E. Machado, M. Cucuzzella, A. J. Malan, J. M. A. Scherpen, and S. Hohmann, "Port-Hamiltonian modeling of hydraulics in 4th generation district heating networks," in *Proc. IEEE 61st Conf. Decis. Control (CDC)*, Dec. 2022, pp. 1182–1189.

[13] K. Sartor, D. Thomas, and P. Dewallef, "A comparative study for simulating heat transport in large district heating network," in *Proc. 28th Int. Conf. Efficiency, Cost, Optim., Simul. Environ. Impact Energy Syst.*, 2015, pp. 1–27.

[14] F. Casella and A. Leva, "Modelling of thermo-hydraulic power generation processes using modelica," *Math. Comput. Model. Dyn. Syst.*, vol. 12, no. 1, pp. 19–33, Feb. 2006.

[15] *ThermoPower Library*. Accessed: Sep. 20, 2024. [Online]. Available: https://github.com/casella/ThermoPower

[16] A. Dahash, S. Mieck, F. Ochs, and H. J. Krautz, "A comparative study of two simulation tools for the technical feasibility in terms of modeling district heating systems: An optimization case study," *Simul. Model. Pract. Theory*, vol. 91, pp. 48–68, Feb. 2019.

[17] Y. Li, Y. Rezgui, and H. Zhu, "Dynamic simulation of heat losses in a district heating system: A case study in Wales," in *Proc. IEEE Smart Energy Grid Eng.*, Aug. 2016, pp. 273–277.

[18] M. Rose, H. Gernandt, J. E. Machado, and J. Schiffer, "Model predictive control of district heating grids using stabilizing terminal ingredients," 2024, *arXiv:2404.01820*.

[19] X. Zheng, Z. Shi, Y. Wang, H. Zhang, and H. Liu, "Thermo-hydraulic condition optimization of large-scale complex district heating network: A case study of Tianjin," *Energy*, vol. 266, Mar. 2023, Art. no. 126406.

[20] M. Taylor, S. Long, O. Marjanovic, and A. Parisio, "Model predictive control of smart districts with fifth generation heating and cooling networks," *IEEE Trans. Energy Convers.*, vol. 36, no. 4, pp. 2659–2669, Dec. 2021.

[21] S. S. Farahani, Z. Lukszo, T. Keviczky, B. De Schutter, and R. M. Murray, "Robust model predictive control for an uncertain smart thermal grid," in *Proc. Eur. Control Conf. (ECC)*, Jun. 2016, pp. 1195–1200.

[22] S. Long, O. Marjanovic, and A. Parisio, "Generalised control-oriented modelling framework for multi-energy systems," *Appl. Energy*, vol. 235, pp. 320–331, Feb. 2019.

[23] F. Verrilli, A. Parisio, and L. Glielmo, "Stochastic model predictive control for optimal energy management of district heating power plants," in *Proc. IEEE 55th Conf. Decis. Control (CDC)*, Dec. 2016, pp. 807–812.

[24] G. Sandou, S. Font, S. Tebbani, A. Hiret, and C. Mondon, "Predictive control of a complex district heating network," in *Proc. 44th IEEE Conf. Decis. Control*, Dec. 2005, pp. 7372–7377.

[25] D. Quaggiotto, J. Vivian, and A. Zarrella, "Management of a district heating network using model predictive control with and without thermal storage," *Optim. Eng.*, vol. 22, no. 3, pp. 1897–1919, Sep. 2021.

[26] M. Wirtz, L. Neumaier, P. Remmen, and D. Müller, "Temperature control in 5th generation district heating and cooling networks: An MILP-based operation optimization," *Appl. Energy*, vol. 288, Apr. 2021, Art. no. 116608.

[27] L. Frison, M. Kollmar, A. Oliva, A. Bürger, and M. Diehl, "Model predictive control of bidirectional heat transfer in prosumer-based solar district heating networks," *Appl. Energy*, vol. 358, Mar. 2024, Art. no. 122617.

[28] A. L. Bella, A. D. Corno, and A. Scaburri, "Data-driven modelling and optimal management of district heating networks," in *Proc. AEIT Int. Annu. Conf. (AEIT)*, Oct. 2021, pp. 1–6.

[29] S. Buffa, A. Soppelsa, M. Pipiciello, G. Henze, and R. Fedrizzi, "Fifth-generation district heating and cooling substations: Demand response with artificial neural network-based model predictive control," *Energies*, vol. 13, no. 17, p. 4339, Aug. 2020.

[30] M. Jiang, M. Speetjens, C. Rindt, and D. Smeulders, "A data-based reduced-order model for dynamic simulation and control of district-heating networks," *Appl. Energy*, vol. 340, Jun. 2023, Art. no. 121038.

[31] E. Terzi, T. Bonetti, D. Saccani, M. Farina, L. Fagiano, and R. Scattolini, "Learning-based predictive control of the cooling system of a large business centre," *Control Eng. Pract.*, vol. 97, Apr. 2020, Art. no. 104348.

[32] L. Wang et al., "Integrated energy system optimal operation using data-driven district heating network model," *Energy Buildings*, vol. 291, Jul. 2023, Art. no. 113100.

[33] C. M. Jensen, M. C. Frederiksen, C. S. Kallesøe, J. N. Jensen, L. H. Andersen, and R. Izadi-Zamanabadi, "HAVOK model predictive control for time-delay systems with applications to district heating," *IFAC-PapersOnLine*, vol. 56, no. 2, pp. 2238–2243, 2023.

[34] L. Boca de Giuli, A. La Bella, and R. Scattolini, "Physics-informed neural network modeling and predictive control of district heating systems," *IEEE Trans. Control Syst. Technol.*, vol. 32, no. 4, pp. 1182–1195, Jul. 2024.

[35] J. Barco-Burgos, J. C. Bruno, U. Eicker, A. L. Saldaña-Robles, and V. Alcántar-Camarena, "Review on the integration of high-temperature heat pumps in district heating and cooling networks," *Energy*, vol. 239, Jan. 2022, Art. no. 122378.

[36] A. Benonysson, B. Bøhm, and H. F. Ravn, "Operational optimization in a district heating system," *Energy Convers. Manage.*, vol. 36, no. 5, pp. 297–314, May 1995.

[37] Y. Wang, S. You, H. Zhang, W. Zheng, X. Zheng, and Q. Miao, "Hydraulic performance optimization of meshed district heating network with multiple heat sources," *Energy*, vol. 126, pp. 603–621, Aug. 2017.

[38] M. Stewart, *Surface Production Operations: Fluid Flow and Pressure Drop*. Houston, TX, USA: Gulf Professional Publishing, 2015.

[39] P. J. Thomas, *Simulation of Industrial Processes for Control Engineers*. Amsterdam, The Netherlands: Elsevier, 1999.

[40] M. Stewart, *Surface Production Operations: Facility Piping and Pipeline Systems*. Houston, TX, USA: Gulf Professional Publishing, 2015.

[41] J. E. Machado, J. Ferguson, M. Cucuzzella, and J. M. A. Scherpen, "Decentralized temperature and storage volume control in multiproducer district heating," *IEEE Control Syst. Lett.*, vol. 7, pp. 413–418, 2023.

[42] L. Saarinen, "Modelling and control of a district heating system," M.S. thesis, Uppsala Univ., Uppsala, Sweden, 2008. [Online]. Available: https://uu.diva-portal.org/smash/record.jsf?pid=diva2%3A461661&dswid=3373

[43] T. Nussbaumer, S. Thalmann, A. Jenni, and J. Ködel, *Handbook on Planning of District Heating Networks*. Bern, Switzerland: Federal Office Energy, 2020.

[44] G. Chicco, S. Riaz, A. Mazza, and P. Mancarella, "Flexibility from distributed multienergy systems," *Proc. IEEE*, vol. 108, no. 9, pp. 1496–1517, Sep. 2020.

[45] H. Bastida, C. E. Ugalde-Loo, M. Abeysekera, M. Qadrdan, J. Wu, and N. Jenkins, "Dynamic modelling and control of thermal energy storage," *Energy Proc.*, vol. 158, pp. 2890–2895, Feb. 2019.

[46] S. E. Mattsson, H. Elmqvist, and M. Otter, "Physical system modeling with modelica," *Control Eng. Pract.*, vol. 6, no. 4, pp. 501–510, Apr. 1998.

[47] P. Fritzson et al., "The OpenModelica integrated environment for modeling, simulation, and model-based development," *Model., Identificat. Control, Norwegian Res. Bull.*, vol. 41, no. 4, pp. 241–295, 2020.

[48] A. Bemporad and M. Morari, "Control of systems integrating logic, dynamics, and constraints," *Automatica*, vol. 35, no. 3, pp. 407–427, 1999.

[49] A. La Bella, A. Falsone, D. Ioli, M. Prandini, and R. Scattolini, "A mixed-integer distributed approach to prosumers aggregation for providing balancing services," *Int. J. Electr. Power Energy Syst.*, vol. 133, Dec. 2021, Art. no. 107228.

[50] C. De Persis and C. S. Kallesoe, "Pressure regulation in nonlinear hydraulic networks by positive and quantized controls," *IEEE Trans. Control Syst. Technol.*, vol. 19, no. 6, pp. 1371–1383, Nov. 2011.

[51] D. B. West et al., *Introduction to Graph Theory*, vol. 2. Upper Saddle River, NJ, USA: Prentice-Hall, 2001.

[52] A. La Bella, L. Nigro, and R. Scattolini, "Predictive control and benefit sharing in multi-energy systems," *IEEE Trans. Control Syst. Technol.*, vol. 32, no. 2, pp. 368–383, Mar. 2024.
[53] B. D. Anderson and J. B. Moore, *Optimal Filtering*. North Chelmsford, MA, USA: Courier Corporation, 2012.
[54] K. Sartor and P. Dewalef, "Experimental validation of heat transport modelling in district heating networks," *Energy*, vol. 137, pp. 961–968, Oct. 2017.
[55] J. A. E. Andersson, J. Gillis, G. Horn, J. B. Rawlings, and M. Diehl, "CasADi: A software framework for nonlinear optimization and optimal control," *Math. Program. Comput.*, vol. 11, no. 1, pp. 1–36, Mar. 2019.
[56] A. Wächter and L. T. Biegler, "On the implementation of an interior-point filter line-search algorithm for large-scale nonlinear programming," *Math. Program.*, vol. 106, no. 1, pp. 25–57, Jul. 2006.

Lorenzo Nigro (Graduate Student Member, IEEE) received the M.Sc. degree in automation and control engineering from the Politecnico di Milano, Italy, in 2022, where he is currently pursuing the Ph.D. degree in information technology. In 2021, he was a Visiting Student with RWTH Aachen University, Aachen, Germany. In 2022, he was a Research Assistant with the Politecnico di Milano, collaborating with the research center Ricerca sul Sistema Energetico (RSE) S.p.A. His research interests include model predictive control, optimization, and the modeling of energy systems, with a particular interest in multi-energy systems and district heating networks. In 2023, he was assigned the Best M.Sc. Thesis Award in sustainability by the IEEE Italy Section.

Alessio La Bella (Member, IEEE) received the B.Sc. and M.Sc. degrees (cum laude) in automation engineering from the Politecnico di Milano in 2013 and 2015, respectively, the integrated Alta Scuola Politecnica Diploma and M.Sc. degree (cum laude) in mechatronics engineering from the Politecnico di Torino in 2016, and the Ph.D. degree (cum laude) in information technology from the Politecnico di Milano in 2020. He was a Visiting Researcher with the Automatic Control Laboratory, École Polytechnique Frale de Lausanne, Switzerland, in 2018, and the Center for Systems and Control, Technische Universiteit Delft, The Netherlands, in 2024. From 2020 to 2022, he was a Research Engineer with Ricerca sul Sistema Energetico (RSE) S.p.A., designing and implementing advanced predictive control systems for district heating networks and large-scale battery plants, in collaboration with industrial companies and energy utilities. In 2022, he joined the Dipartimento di Elettronica, Informazione e Bioingegneria, Politecnico di Milano, as an Assistant Professor. His research interests include the theory and design of predictive, multi-agent, and learning-based control systems, with a particular emphasis on practical challenges arising from the upcoming energy transition. He was a recipient of the Dimitris N. Chorafas Prize in 2020. He is an Associate Editor of the *International Journal of Adaptive Control and Signal Processing* and the EUCA Conference Editorial Board.

Francesco Casella (Member, IEEE) received the master's degree (cum laude) in electronic engineering and the Ph.D. degree in information and control science from the Politecnico di Milano. He is currently an Associate Professor of Control Systems and Advanced Process Control with the Politecnico di Milano. In recent years, he has worked in publicly and privately funded research projects involving innovative thermal generation power plants and gas transportation networks. He has published over 150 journal articles and conference papers, mostly on these topics. His main research interests include modeling and control of energy systems, and equation-based and object-oriented modeling of engineering systems at large. He is a member of the Board of the Modelica Association. He is the Director of the Open Source Modelica Consortium, which develops the OpenModelica modeling and simulation software.

Riccardo Scattolini is currently a Full Professor of Automatic Control with the Politecnico di Milano, Italy. His main research interests include modeling, identification, simulation, diagnosis, and control of industrial plants and energy systems, with an emphasis on theory and applications of model predictive control and fault detection methods to large-scale and networked systems. He was awarded the Heaviside Premium of the Institution of Electrical Engineers, U.K. He was an Associate Editor of *Automatica* (IFAC).

Open Access funding provided by 'Politecnico di Milano' within the CRUI CARE Agreement